國 立 交 通 大 學

機械工程學系
碩 士 論 文

二維微步進機構定位之研究

The Research of Positioning for

Two-Dimension Micro-stepping Mechanism

研 究 生：鄧明欣

指導教授：成維華　教授

中華民國九十六年七月

二維微步進機構定位之研究

The Research of Positioning for

Two-Dimension Micro-stepping Mechanism

研 究 生：鄧明欣　　　　　　Student：Ming-Shin Deng

指導教授：成維華　　　　　　Advisor：Wei-Hua Chieng

國 立 交 通 大 學

機 械 工 程 學 系

碩 士 論 文

A Thesis

Submitted to Institute of Mechanical Engineering

College of Engineering

National Chiao Tung University

in partial Fulfillment of the Requirements

for the Degree of

Master

in

Mechanical Engineering

July 2007

Hsinchu, Taiwan, Republic of China

中華民國九十六年七月

二維微步進機構定位之研究

研究生：鄧明欣　　　　　　　　　指導教授：成維華　教授

國立交通大學機械工程學系

摘要

壓電致動器具有低能量消耗、高精準度和反應時間短等優點，壓電致動器對於微步進機構是一種相當好的驅動器，微步進機構是利用壓電致動器對應驅動電壓反應快速的特性及黏滯與滑動的摩擦機制，建構出可以用於精密定位的衝量驅動機構。在此我們選用質量-阻尼-彈簧之衝量驅動機構來分析此機構的動力學。實驗則分為兩部分，首先利用 DSP 控制器與雷射干涉儀量測系統來進行實驗，以探討不同的壓電致動器對應相同的驅動波形使機構產生步進現象有何差異，並同時對壓電致動器與微步進機構進行系統鑑別。然後再進行二維微步進機構之平移與旋轉實驗，來探討不同的驅動電壓與機構移動的方式之間的關係，進一步使二維微步進機構的移動與期望的結果相符，以達到精密定位的目的。

The Research of Positioning for
Two-Dimension Micro-stepping Mechanism

Student：Ming-Shin Deng   Advisor：Dr. Wei-Hua Chieng

Institute of Mechanical Engineering
National Chiao Tung University

Abstract

Because of low power consumption, ultra-high resolution and rapid response, piezoelectric actuator is one better choice of actuator for micro-stepping mechanism. Micro-stepping mechanism is an impact drive mechanism constructed by using the rapid displacement response of piezoelectric actuator and stick-slip motion of friction mechanism. A mass-damper-spring model is constructed to investigate the dynamics of the mechanism. The experiments are divided into two sections. We will combine the DSP controller and the laser interferometer measuring system to the experiment. To discuss the influences of different piezoelectric actuators and to identify the system of micro-stepping mechanism will help us to begin the next experiment. Next experiment is about the shift and rotation of 2-dimension micro-steeping. To find out the relations between the different waveforms and the displacement of the mechanism is the way to make the result close to the simulation and to achieve the purpose of precise positioning.

誌謝

首先, 我要感謝我的指導老師，成維華教授。在我唸研究所的期間，老師在課業跟生活等方面，都給我許多很寶貴的意見，讓我獲益良多。我還要感謝那些曾經幫助我的人，包括張國樑學長、葛雷學長、黑人學長等，還有一起走過這兩年風風雨雨的同學們，偉鈞、建成、侯兄以及曹兄。還有製造熱鬧的學弟們，強哥、洋豪、文彬以及小賴。還有那些曾經協助過我的人。最後我要感謝我的家人跟我的女友，因為沒有他們的支持就沒有今天的我。

Contents

List of figures

List of Tables

Chapter 1 Introduction

1.1 History

Many types of piezoelectric precision positioning systems have been proposed for industrial and scientific applications. Figure 1.1 lists the typical classifications of these systems. Scanning devices produce motion by direct driven or mechanical amplified. Pulse devices include stick-slip and other types of clamping mechanism. The stick-slip device which is based on the rapid response of continuous driving voltage can generate stable stepping motion from mechanical excitation of the piezoelectric device. The stick-slip behavior results from the contact friction between the movable part and the guide surface. The third type of piezoelectric positioning system is the ultrasonic motor. The acoustic wave produced by resonantly excite piezoelectric materials induces the mechanical movement.

The pulse device seems to solve the problem of limited stroke of the scanning device. However, some bottlenecks remain.

(1) The load capacity of the pulse device, especially the stick-slip device, is low. The load variation dramatically changes the behavior of the mechanism.

(2) The stick-slip is sensitive to changes in the surroundings, such as the indeterminate distribution of friction on the guide surface, the tilting of the guide surface and mechanical vibration.

(3) The closed loop operation of the stick-slip device has not been

well developed. Current applications of stick-slip devices are based on open loop operation.

(4) The mechanism and controller must be carefully designed. A stick-slip device operated at high frequency will be out of control in a poorly damped system.

Although several disadvantages affect the application of stick-slip devices, their simple structure and effective precise positioning are the main object of the research.

The development of impact drive mechanism began with the design of a finely adjustable specimen holder for SEMs/STMs in the 1980s. T. Higuchi et al. proposed a prototype IDM and applied it in the design of a micro robot that serves as an inserted capillary in a cell-operation [2]. Simplified kinematics analysis was performed and the basic principle of operation of IDM was thus elucidated. S. Ling et al. used MCK model to study numerically a push-pull IDM [2]. They treated IDM simply as a velocity drive and considered only the effect of the amplitude and the frequency of input waveform on the mean velocity of IDM. All of the analysis and simulation was based on a specific IDM construction. The design parameters of IDM and the induced stepping behavior of IDM were thoroughly analyzed.

The stick-slip operation of IDM is dominated by the energy dissipation of the system, some of which results from the contact friction between the slider and the guide surface. K. Furutani et al. studied the effect of lubrication on IDM [4]. They discussed the motion of IDM based on Newton mechanics. An approximate estimate of the motion of IDM under a specific exciting waveform pattern was provided. Four

guide-surface conditions – dry, lubricated by EDF-K, Oil 32 and Oil 68 – were experimentally studied. Surface condition did not apparently affect the behavior of IDM. The critical effect of the dissipation of energy in the system is not discussed.

The application of IDM to multi D.O.F. positioning has also been extensively discussed. J. Mendes et al. constructed a planar positioning machine to finely position a print board on a work plane [3]. They used a group of six IDMs in a plane to push a wok piece in the X and Y directions. The path planning of the work piece which uses six actuators was performed. Image feedback was used to achieve closed-loop position control. The mechanism was based on the robotic "Pushing Operation" of M. Mason et al. [5][6][8]. Y. Yamagata et al. proposed a similar approach [7]. They used a multi D.O.F. IDM on the end effecter of a robot arm to perform automatic, precise assembly. K. Furutani et al. used IDM to develop a precision electrical discharge machine (EDM) [9][10]. They constructed an X-Y-Z-θ movable electrode-feeding device. The electrode was carried with the planar IDM. The path planning of the planer IDM-driven electrode was also accomplished.

Many clamping mechanisms were introduced to "increase" the friction force between the slider and the guide surface during the "sticking phase" of the operation of IDM to improve the poor controllability and repeatability of the stick-slip motion. K. Ikuta et al. proposed a kind of IDM using electromagnetic clamping [11]. The slider is electromagnetically clamped during the sticking phase and released during the slip phase. An extra D.O.F. of control of the electromagnetic coil was introduced. T. Idogaki et al. used a preload spring to clamp the

slider to the guide surface of IDM [12]. The passive preload exerts a larger normal force between the contact surface of the slider and the guide of IDM.

The piezoelectric material-based IDM was selected as the precise positioning in this research. The following sections emphasize on the operation and stepping behavior of IDM.

1.2 Motive

In recent decades the needs and uses of precise positioning devices extend from mechanical field to the communication field to the military applications and the automotive field. Precise positioning has been incorporated into production processes in mining, agriculture and construction. The main application has been in machine guidance and machine automation which require high levels of precision. Precise Positioning is also increasingly used in the fields of robotics. Because of these reason, we have to find precise positioning devices that can be more accurate.

1.3 Research Orientation

By the requirement of precision the scale of motion of micro-stepping mechanism must be decreased. We must solve some problems to achieve the goal.

Our mechanism is a modified impact drive mechanism (IDM) which

belongs to the stick slip device of pulse type. The operating principle of IDM is to apply asymmetric voltage waveform to PZT which is connected to slider and counter-mass of IDM and then the IDM causes a series of stick-slip motion on the guide way. A mass-damper-spring model combined with friction model is adopted to investigate the dynamics of the mechanism.

An experiment environment, base on the laser interferometer, is set up for measuring the displacement of micro-stepping mechanism. After the data converting reference and the measurement signals is read from the laser and the measurement receiver, the information is processed by DSP. The DSP module can also produce the driving waveforms needed in the experiment at the same time. By comparing the results of experiment and simulation we can know if the models of micro-stepping mechanism are suitable.
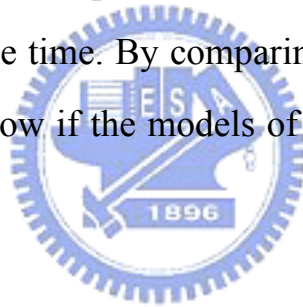
Chapter 2 Model of 1-D IDM

2.1 Operating Principle of Impact Drive Mechanism

Figure 2.1 describes the input waveform pattern corresponding to the movement of one dimensional linear positioning device. The slider is put on a surface and held by the friction force. A counter-mass is connected to the main object via one piezoelectric element. Controlling extension or contraction of the piezoelectric actuator by applying voltage waveforms to the piezoelectric actuator, the mechanism will move step by step. Figure 2.1(a) represents a control method of deformations of the piezoelectric actuator for backward movement.

(1) A movement cycle begins with the original length of the piezoelectric actuator and the mechanism is stationary at start.

(2) A steep rising voltage is applied. The piezoelectric actuator makes a rapid extension and the slider moves backward and the counter-mass forward.

(3) While returning, the counter-mass should be accelerated by a constant acceleration which causes inertial force less than the static friction force. Otherwise, the slider makes reverse movement.

(4) By the time the piezoelectric actuator is contracted to the length of the beginning, a sudden stop is happened. This action is just like a collision of the counter-mass and the slider. So the whole system starts moving backward against friction force until it loses its kinetic energy.

(5) IDM stops and the piezoelectric actuator recovers itself.

The cycle is completed through (1) to (5). Therefore, IDM can move a long distance by repeating this cycle. The same may be said, no doubt, of forward movement as shown in Figure 2.1(b).

(1) A movement cycle begins with the original length of the piezoelectric actuator and the mechanism is stationary at start.

(2) A gentle rising voltage is applied. The piezoelectric actuator makes a extension and the slider moves backward and the counter-mass forward.

(3) While returning, the counter-mass should be accelerated by a constant acceleration which causes inertial force less than the static friction force. Otherwise, the slider makes reverse movement.

(4) By the time the piezoelectric actuator is elongated, a sudden stop is happened. Then a steep decreasing voltage is applied. This action which happened in the moment of change of applied voltage is just like a hammer to hit the slider. So the whole system starts moving forward against friction force until it loses its kinetic energy.

(5) IDM stops and the piezoelectric actuator recovers itself.

These all above are the operation of one-dimensional impact drive mechanism about how to move forward and backward. It is similar to the two-dimensional impact drive mechanism. The difference between one-dimension IDM and two-dimension is that the same asymmetrical triangle voltage waveform applied to one-dimension can produce linear movement only, but it applied to two-dimension IDM can produce translative and rotational movement. So we want to control the movement of the two-dimension IDM, we need to know the difference between three actuators about the same and different input waveform

2.2 The mass-damper-spring model of 1-D IDM

In usual case, F_1 is frictional force F_μ and F_2 is equal to zero. The mass-damper-spring model of IDM shown in Figure 2.2 is expressed as follows:

$$\begin{cases} M\ddot{x}_1 + c\left(\dot{x}_1 + \dot{l} - \dot{x}_2\right) + k\left(x_1 + l - x_2\right) = F_\mu \\ m\ddot{x}_2 + c\left(\dot{x}_2 - \dot{l} - \dot{x}_1\right) + k\left(x_2 - l - x_1\right) = 0 \end{cases} \tag{2.1}$$

The piezoelectric actuator is considered to be linear and rigid. According to the design of the piezoelectric actuator, the mechanical interface between the slider and the counter-mass is specified as a linear spring constant k and a linear damping coefficient c. Assuming no contact friction between the counter-mass and the guide way, there is only one friction between the slider and the guide way. The variables x_1, x_2, l represent the displacement of the slider, the counter-mass and the piezoelectric actuator respectively; M and m are the mass of the slider and the counter-mass.
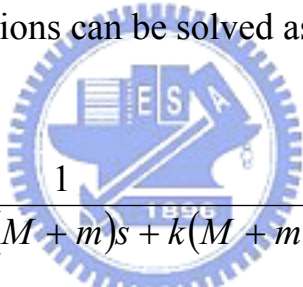
In a more general case, external forces act on the slider and the counter-mass (frictional force, magnetic clamping force, etc.), the mass-damper-spring model for the system turns into

$$\begin{cases} M\ddot{x}_1 + c\left(\dot{x}_1 + \dot{l} - \dot{x}_2\right) + k\left(x_1 + l - x_2\right) = F_1 \\ m\ddot{x}_2 + c\left(\dot{x}_2 - \dot{l} - \dot{x}_1\right) + k\left(x_2 - l - x_1\right) = F_2 \end{cases} \tag{2.2}$$

where F_1 and F_2 represent the external force on the slider and the counter-mass respectively. By taking the Laplace transform for both sides of above equations, we have

$$\left(Ms^2 + cs + k\right)X_1(s) - \left(cs + k\right)X_2(s) = -\left(cs + k\right)L(s) + F_1(s)$$
$$+ M\left(sx_1(0) + \dot{x}_1(0)\right) + c\left(x_1(0) - x_2(0) + l(0)\right)$$
$$-\left(cs + k\right)X_1(s) + \left(ms^2 + cs + k\right)X_2(s) = \left(cs + k\right)L(s) + F_2(s)$$
$$+ m\left(sx_2(0) + \dot{x}_2(0)\right) + c\left(x_2(0) - x_1(0) - l(0)\right)$$

(2.3)

The above algebraic equations can be solved as

$$\begin{bmatrix} X_1 \\ X_2 \end{bmatrix} = \frac{1}{s^2\left(Mms^2 + c(M+m)s + k(M+m)\right)}$$
$$\cdot \begin{bmatrix} ms^2 + cs + k & cs + k \\ cs + k & Ms^2 + cs + k \end{bmatrix} \begin{bmatrix} -\left(cs + k\right)L + F_1 + I_1 \\ \left(cs + k\right)L + F_2 + I_2 \end{bmatrix}$$

(2.4)

Where $I_1 = Mx_1(0)s + I_{10}$ and $I_2 = mx_2(0)s + I_{20}$ represents the terms which contain the initial conditions of the system. We can rewrite the vector $\begin{bmatrix} X_1 & X_2 \end{bmatrix}^T$ composed of 5 separated vectors.

$$\begin{bmatrix} X_1 \\ X_2 \end{bmatrix} = \begin{bmatrix} X_{1,L} \\ X_{2,L} \end{bmatrix} + \begin{bmatrix} X_{1,F1} \\ X_{2,F1} \end{bmatrix} + \begin{bmatrix} X_{1,F2} \\ X_{2,F2} \end{bmatrix} + \begin{bmatrix} X_{1,I1} \\ X_{2,I1} \end{bmatrix} + \begin{bmatrix} X_{1,I2} \\ X_{2,I2} \end{bmatrix}$$

(2.5)

Where subscript L, $F1$ and $F2$ represent the effect of piezoelectric

9

element, external forces act on the slider and the counter-mass. *I*1 and *I*2 represent the effect of the initial conditions of the system. The individual quantity can be obtained as follows.

$$
\begin{cases}
X_{1,L} = \dfrac{-m(cs+k)\cdot L(s)}{Mms^2 + c(M+m)s + k(M+m)} = G_{L1}(s)L(s) \\[4mm]
X_{2,L} = \dfrac{M(cs+k)\cdot L(s)}{Mms^2 + c(M+m)s + k(M+m)} = G_{L2}(s)L(s)
\end{cases}
\tag{2.6}
$$

$$
\begin{cases}
X_{1,F1} = \dfrac{(ms^2+cs+k)\cdot F_1(s)}{s^2\left(Mms^2 + c(M+m)s + k(M+m)\right)} = G_{F11}(s)F_1(s) \\[4mm]
X_{2,F1} = \dfrac{(cs+k)\cdot F_1(s)}{s^2\left(Mms^2 + c(M+m)s + k(M+m)\right)} = G_{F12}(s)F_1(s)
\end{cases}
\tag{2.7}
$$

$$
\begin{cases}
X_{1,F2} = \dfrac{(cs+k)\cdot F_2(s)}{s^2\left(Mms^2 + c(M+m)s + k(M+m)\right)} = G_{F21}(s)F_2(s) \\[4mm]
X_{2,F2} = \dfrac{(Ms^2+cs+k)\cdot F_2(s)}{s^2\left(Mms^2 + c(M+m)s + k(M+m)\right)} = G_{F22}(s)F_2(s)
\end{cases}
\tag{2.8}
$$

$$
\begin{cases}
X_{1,I1} = \dfrac{(ms^2+cs+k)\cdot (Mx_1(0)s + I_{10})}{s^2\left(Mms^2 + c(M+m)s + k(M+m)\right)} \\[4mm]
X_{2,I1} = \dfrac{(cs+k)\cdot (Mx_1(0)s + I_{10})}{s^2\left(Mms^2 + c(M+m)s + k(M+m)\right)}
\end{cases}
\tag{2.9}
$$

$$
\begin{cases}
X_{1,I2} = \dfrac{(cs+k)\cdot (mx_2(0)s + I_{20})}{s^2\left(Mms^2 + c(M+m)s + k(M+m)\right)} \\[4mm]
X_{2,I2} = \dfrac{(Ms^2+cs+k)\cdot (mx_2(0)s + I_{20})}{s^2\left(Mms^2 + c(M+m)s + k(M+m)\right)}
\end{cases}
\tag{2.10}
$$

By the inverse Laplace transform $L^{-1}\{\cdot\}$ the displacement of the slider

under actuation of IDM can be obtained as

$$x_1(t) = L^{-1}\{G_{L1}(s)L(s)\} + L^{-1}\{G_{F11}(s)F_1(s)\} + L^{-1}\{G_{F21}(s)F_2(s)\}$$

$$+ L^{-1}\{X_{1,I1}(s)\} + L^{-1}\{X_{2,I2}(s)\} \tag{2.11}$$

In the following formulations, we assume the load capacity of piezoelectric element is large enough and the output is corresponding to the rapid deflection stage or the slow deflection stage of the piezoelectric element only. The displacement of slider drive previously can be rewritten as

$$x_{1,L} = \frac{mL_{max}\,sin\varpi_d t \cdot e^{-\xi\varpi_n t}}{\beta T(M+m)\varpi_d} - \frac{mL_{max}}{M+m}\frac{t}{\beta T} \tag{2.12}$$

$$x_{2,L} = \frac{-ML_{max}\,sin\varpi_d t \cdot e^{-\xi\varpi_n t}}{\beta T(M+m)\varpi_d} + \frac{ML_{max}}{M+m}\frac{t}{\beta T} \tag{2.13}$$

where β represents the percentage of the slanting stage in a cycle (γ or $1-\gamma$); L_{max} represents the maximum deflection of the piezoelectric element; γ and T depicted in Figure 2.7 are the complement duty cycle and the period of triangular waveform respectively. Similarly, we can obtain the relation between the displacement of the slider and external constant forces F_1 and F_2 as follows.

$$x_{1,F1}(t) = \left\{ \left[\frac{-cm\sin\varpi_d t}{2kM(M+m)\varpi_d} - \frac{m^2\cos\varpi_d t}{k(M+m)^2} \right] \cdot e^{-\xi\varpi_n t} + \frac{m^2}{k(M+m)^2} + \frac{t^2}{2(M+m)} \right\} F_1$$

$$x_{2,F1}(t) = \left\{ \left[\frac{c\sin\varpi_d t}{2k(M+m)\varpi_d} + \frac{Mm\cos\varpi_d t}{k(M+m)^2} \right] \cdot e^{-\xi\varpi_n t} - \frac{Mm}{k(M+m)^2} + \frac{t^2}{2(M+m)} \right\} F_1$$

$$x_{1,F2}(t) = \left\{ \left[\frac{c\sin\varpi_d t}{2k(M+m)\varpi_d} + \frac{Mm\cos\varpi_d t}{k(M+m)^2} \right] \cdot e^{-\xi\varpi_n t} - \frac{Mm}{k(M+m)^2} + \frac{t^2}{2(M+m)} \right\} F_2$$

$$x_{2,F2}(t) = \left\{ \left[\frac{-Mc\sin\varpi_d t}{2km(M+m)\varpi_d} - \frac{M^2\cos\varpi_d t}{k(M+m)^2} \right] \cdot e^{-\xi\varpi_n t} + \frac{M^2}{k(M+m)^2} + \frac{t^2}{2(M+m)} \right\} F_2$$

Finally, the initial condition of slider displacement and counter-mass displacement for each stage are

$$x_{1,I1}(t) = \left[\frac{2mI_{10} - c(M+m)x_1(0)}{2M(M+m)\varpi_d}\sin\varpi_d t + \frac{mx_1(0)}{M+m}\cos\varpi_d t \right] e^{-\xi\varpi_n t} + \frac{Mx_1(0) + I_{10}t}{M+m}$$

$$x_{2,I1}(t) = \left[\frac{c(M+m)x_1(0) - 2mI_{10}}{2m(M+m)\varpi_d}\sin\varpi_d t - \frac{Mx_1(0)}{M+m}\cos\varpi_d t \right] e^{-\xi\varpi_n t} + \frac{Mx_1(0) + I_{10}t}{M+m}$$

$$x_{1,12}(t) = \left[\frac{c(M+m)x_2(0) - 2MI_{20}}{2M(M+m)\varpi_d} \sin\varpi_d t - \frac{mx_2(0)}{M+m} \cos\varpi_d t \right] e^{-\xi\varpi_n t} + \frac{mx_2(0) + I_{20}t}{M+m}$$

$$x_{2,12}(t) = \left[\frac{2MI_{20} - c(M+m)x_2(0)}{2m(M+m)\varpi_d} \sin\varpi_d t + \frac{Mx_2(0)}{M+m} \cos\varpi_d t \right] e^{-\xi\varpi_n t} + \frac{mx_2(0) + I_{20}t}{M+m}$$

From above formulation, we can conclude the characteristic of IDM as a second order dynamic system with damped natural frequency and damping ratio as follows.

$$\varpi_d = \varpi_n\sqrt{1-\xi^2} = \frac{1}{2Mm}\sqrt{(M+m)[4kMm - c^2(M+m)]} \quad (2.14)$$

$$\xi\varpi_n = \frac{c(M+m)}{2Mm} \quad (2.15)$$

$$\xi = \frac{c(M+m)}{\sqrt{4kMm(M+m)}} = \frac{c}{2}\sqrt{\frac{M+m}{kMm}} \quad (2.16)$$

2.3 System Identification of 1-D IDM Model

The parameters of the proposed model must be estimated from the experimentally measured data to predict the behavior of the mechanism precisely enough. As described in the preceding sections, a model of IDM with a linearized MCK system consists of a Coulomb friction model and a linear actuator; three parameters are required. The estimated parameters include the stiffness k, the damping coefficient c of the piezoelectric

actuator and the frictional coefficient μ. First we use the model like Figure 2.3 to estimate the stiffness and the damping coefficient. A finite difference approximation to the MCK system is used to discretize the dynamics of the slider and the count-mass of the mechanism. The discretized system is specified as follows.

$$\left(x_i - 2x_{i-1} + x_{i-2}\right) + \frac{c}{m}\Delta\left(x_i - x_{i-1} - u_i + u_{i-1}\right) + \frac{k}{m}\Delta^2\left(x_i - u_i\right) = 0 \quad (2.17)$$

Then the equation of the discretized system can be rearranged as follows.

$$Hw - y = 0$$
$$where \begin{cases} H = \left[x_i - x_{i-1} - u_i + u_{i-1} \quad x_i - u_i\right] \\ w = \left[\frac{c}{m}\Delta \quad \frac{k}{m}\Delta^2\right]^T \\ y = -\left(x_i - 2x_{i-1} + x_{i-2}\right) \end{cases} \quad (2.18)$$

A weighted least square algorithm is used to make sure that the identified parameters properly converge to a range. w is the a matrix that contain the parameters what we want to estimate. The final goal is to estimate the stiffness and the damping coefficient by iteration of w and then minimizing the value of $\|Hw - y\|$. The equations of WRLS are shown as follows:

$$\min_w \|Hw - y\| \quad (2.19)$$

$$P_i = \lambda_i \left[P_{i-1} - \frac{P_{i-1} h_i^* h_i P_{i-1}}{\lambda_i + h_i P_{i-1} h_i^*} \right], P_o = I$$

$$w_i = w_{i-1} + \frac{P_{i-1} h_i^*}{\lambda_i + h_i P_{i-1} h_i^*} (y_i - h_i w_{i-1})$$

λ_i is equal to 0.99 to perform a forgetting factor for the system identification

    The result of parameter estimation is shown as Figure2.5. The upper diagram of Figure 2.4 is the input of actuator and the lower is the output. The stiffness is about 10^7 and the damping coefficient is 200.

2.4 Simulations

    Simulink is a platform for multidomain simulation and Model-Based Design for dynamic systems. It provides an interactive graphical environment and a customizable set of block libraries, and can be extended for specialized applications. We simulate the mass-damper-spring model by the Simulink. The rules of connection follow the equations of the mass-damper-spring model. The results of simulation are shown as Figure 2.6.

Chapter 3 Model of 2-D IDM

3.1 The mass-damper-spring model of 2-D IDM

This model is derived by lagrange method. Lagrange's equation are fundamental relation in Lagrange's mechanics given by

$$\frac{d}{dt}\left(\frac{\partial L}{\partial \dot{q}_l}\right) - \frac{\partial L}{\partial q_l} + \frac{\partial D}{\partial \dot{q}_j} = Q_j \qquad (3.1)$$

where q_j is a general coordinate, Q_j is the general work, D is the energy absorbed by damper and L is the Lagrangian.

$$L \equiv T - U \qquad (3.2)$$

where T is the total kinetic energy and U is the total potential energy.

The kinetic energy include the energy resulted from the movement of the plate and the three count-mass. Based on our assumption the terms of energy are shown as follows behind calculation.

$$
\begin{aligned}
T &= \frac{1}{2}M\dot{x}^2 + \frac{1}{2}M\dot{y}^2 + \frac{1}{2}I\dot{\theta}^2 + \sum_i \frac{1}{2}m_i\left(\dot{x}^2 + \dot{y}^2\right) + \sum_j \frac{1}{2}m_i\left(\dot{d}_i - R_i\dot{\theta}\right)^2 \\
&\quad + \sum_i m_i\left(\dot{d}_i - R_i\dot{\theta}\right)\left[\dot{x}\sin(\phi_i + \theta) - \dot{y}\cos(\phi_i + \theta)\right] \\
U &= \sum_i \frac{1}{2}k_i\left(d_i - u_i\right)^2 \\
&\quad \sum_i \frac{1}{2}c_i\left(\dot{d}_i - \dot{u}_i\right)^2
\end{aligned}
$$

$$ (3.3) $$

To substitute the three terms into the equation 3.1 and to calculate the equations can make us to obtain the model of IDM. The mass-damper-spring model of IDM shown in Figure 3.1 is expressed as follows:

$$
\begin{cases}
M\ddot{x} + \sum_i m_i \ddot{x} + \sum_i m_i (\ddot{d}_i - R_i \ddot{\theta}) \sin(\theta + \phi_i) + \sum_i m_i (\dot{d}_i \dot{\theta} - R_i \dot{\theta}^2) \cos(\theta + \phi_i) = F_{\mu x} \\
M\ddot{y} + \sum_i m_i \ddot{y} - \sum_i m_i (\ddot{d}_i - R_i \ddot{\theta}) \cos(\theta + \phi_i) + \sum_i m_i (\dot{d}_i \dot{\theta} - R_i \dot{\theta}^2) \sin(\theta + \phi_i) = F_{\mu y} \\
I\ddot{\theta} - \sum_i m_i R_i (\ddot{d}_i - R_i \ddot{\theta}) - \sum_i m_i \ddot{x} R_i \sin(\theta + \phi_i) + \sum_i m_i \ddot{y} R_i \cos(\theta + \phi_i) \\
\qquad\qquad - \sum_i m_i \ddot{x} \dot{d}_i \cos(\theta + \phi_i) - \sum_i m_i \ddot{y} \dot{d}_i \sin(\theta + \phi_i) = M_\mu \\
m_i \ddot{x} \sin(\theta + \phi_i) - m_i \ddot{y} \cos(\theta + \phi_i) + m_i \ddot{x} \dot{d}_i \cos(\theta + \phi_i) + m_i \ddot{y} \dot{d}_i \sin(\theta + \phi_i) \\
\qquad\qquad + m_i \ddot{d}_i - m_i R_i \ddot{\theta} + c_i (\dot{d}_i - \dot{u}_i) + k_i (d_i - u_i) = 0
\end{cases}
$$

$$(3.4)$$

in which the Coulomb frictional force and moment between the slider and guide surface can represented as:

$$
\begin{aligned}
F_{\mu x} &= -\frac{\dot{x}}{\sqrt{\dot{x} + \dot{y}}} \mu \left(M + \sum_i m_i \right) g \\
F_{\mu y} &= -\frac{\dot{y}}{\sqrt{\dot{x} + \dot{y}}} \mu \left(M + \sum_i m_i \right) g \\
M_\mu &= -\frac{2}{3} R \, sign(\dot{\theta}) \mu \left(M + \sum_i m_i \right) g
\end{aligned}
$$

$$(3.5)$$

Because the affect of the terms about Coriolis Force is not obvious, these equations can be rearranged as follows:

$$
\begin{cases}
M\ddot{x} + \sum_i m_i\ddot{x} + \sum_i m_i\left(\ddot{d}_i - R_i\ddot{\theta}\right)sin(\theta + \phi_i) = F_{\mu x} \\
M\ddot{y} + \sum_i m_i\ddot{y} - \sum_i m_i\left(\ddot{d}_i - R_i\ddot{\theta}\right)cos(\theta + \phi_i) = F_{\mu y} \\
I\ddot{\theta} - \sum_i m_i R_i\left(\ddot{d}_i - R_i\ddot{\theta}\right) - \sum_i m_i\ddot{x}R_i\,sin(\theta + \phi_i) + \sum_i m_i\ddot{y}R_i\,cos(\theta + \phi_i) = M_\mu \\
m_i\ddot{x}\,sin(\theta + \phi_i) - m_i\ddot{y}\,cos(\theta + \phi_i) + m_i\ddot{d}_i - m_i R_i\ddot{\theta} \\
\qquad\qquad\qquad\qquad + c_i\left(\dot{d}_i - \dot{u}_i\right) + k_i\left(d_i - u_i\right) = 0
\end{cases}
$$

$$(3.6)$$

According to the assumption in section 2.2, the mechanical interface between the slider and the counter-mass is specified as a linear spring constant k_i and a linear damping coefficient c_i. There is no contact friction between the counter-mass and the guide surface but the slider and guide surface. The variables x, y represent the displacements of the mechanism in X-axis and Y-axis. θ represents the rotation of the mechanism. ϕ_i represents the angle between the place where the actuator fastened on and the X'-axis. u_i and d_i are the inputs and the displacement of count-mass respect to the mechanism.

The first three equations are dynamic equations and the others are constraints. These equations are very complicated and nonlinear and cannot be decoupled. It is very difficult to solve these equations directly but numerical methods seem to be better way to solve these equations. To analyze the dynamics of the 2-D micro-stepping mechanism by numerical method need accurate data including the stiffness k_i, damping coefficient c_i of the actuators, the frictional coefficient μ between the mechanism and guide surface and so on. Those data need to be estimated by a series of experiments.

3.2 Simulation of 2-D IDM Model

The simulations of the mass-damper-spring model of 2-D IDM are also by Simulink. The block diagram of the 2-D IDM is shown as Figure 3.2. The block diagram of equation about X-axis is shown as Figure 3.3. The diagram consist of three parts included three inputs in one subsystem, three dynamics equations in three subsystems, three constraint equations in three subsystems. This method of connection will cause a problem, algebraic loop. It can solve the problem by using Runge-Kutta method and setting the step size very small. The parameters of simulation are shown in table 3.1. The results of simulation are shown as Figure 3.4 to Figure 3.6.
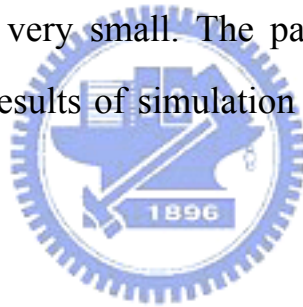
Chapter 4 Experiment

4.1 Experimental Setup of 1-D IDM Model

4.1.1 Input and Measuring System

Figure 4.1 show the sketch of the 1-D IDM. Figure 4.2 and Figure 4.3 depict the overall structure and configuration with actual instrument for measuring the displacement of the piezoelectric actuator respectively. The photograph of the system and IDM are also presented in Figure 4.4 and figure 4.5 In the experiment, the HP10705A interferometer with 10nm(0.4μin) resolution and 3MHz maximum data update rate measures the actual displacement of IDM. The sampling time of the data is controlled by DSP module and then sent to HP10885A. The primary function of The HP10885A Axis board is to convert reference and measured signals from a HP5517C laser head and measurement receiver to a 32-bit digital position word. The unit of measurement associated with the position word is a fraction of the wavelength of the laser light being used. A conversion is required if the position must be known in some other units(mm, inch, etc.).

After conversion, the raw data is read by DSP module directly. The main function of the DSP module are：

(1) To send signals to HP10885A to control the sequence of data sample and hold (8 bits digital output)；

(2) To do data reading (32 bits digital input) ；

(3) To produce driving voltage waveforms needed in the experiment (8 bits DA) and send to IDM.

We achieve this goal by utilizing code compose studio (CCS) software to integrate these tasks into a program which can be loaded to DSP controller. Because of low driving voltage waveforms from DSP module (8 bits DA), a voltage amplifier is needed to amplify the analog signal from 0~2V to 0~100V to drive the piezoelectric actuator. Table 4.1 lists the specifications of the piezoelectric actuator which we used. The inputs of the experiments are shown as Figure 4.17 to Figure 4.19. The frequency and duty ratio of inputs are 300Hz and 95%.

4.1.2 DSP Program Flowchart

The 2407A DSP controllers shown in figure 4.6 are designed to meet the needs of control-based applications. By integrating the high performance of a DSP core and the on-chip peripherals of a microcontroller into a single-chip solution, the 240xA series yields a device that is an affordable alternative to traditional microcontroller units (MCUs) and expensive multichip designs. At 40 million instructions per second (MIPS), the 2407A DSP controllers offer significant performance over traditional 16-bit microcontrollers and microprocessors. The 16-bit, low power, fixed-point DSP core of the 2407A device provides analog designers a digital solution that does not sacrifice the precision and performance of their systems. See details in Figure 4.7.

Code composer studio (CCS) is a fully software integrated development environment (IDE) for building and debugging programs for the DSK (DSP Starter Kit), i.e. the DSP board. CCS integrates all host and target tools in a unified environment to simplify DSP system configuration and application design. This easy to use development environment allows DSP designers of all experience levels full access to all phases of the code development process. The software is used for three phases in the overall DSP system design process:

(1)Coding and building: writing code using the editor, creating a 'project', and compiling and linking.

(2)Debugging: syntax checking, probe points, break points

(3)Analysis: statistics, benchmarking, real-time debugging

Figure 4.8 describes the complete flowchart of the DSP program. The processes are as follows:

(1) Start: The program starts.

(2) CPU will be initialized first. Then we set and enable time interrupt to define the sampling time.

(3) A while loop for DA control waveforms applying to the piezoelectric actuator is executed. The program waits for the time interrupt every 50 us (sampling rate = 20kHz).

(4) The program gets into time interrupt, the DSP module starts to read data by 32bits digital input.

(5) MSB Check: Because we do not know if an error occurs, the received data has to be checked first if an error occurs. The method provided from operating manual is to examine the most significant bit (MSB). If the MSB is one (true), it implies the data is correct. Otherwise,

there exists an error. We should adjust all the experiments of the laser interferometer and see if the light status is ready especially the indicator of the receiver. Then restart the program again to step (1).

(6) Sign Check: The meaning of the second MSB indicates the sign of the position value; therefore it is sometimes called the sign bit. The sign bit zero (false) means positive and one (true) means negative position. Negative position needs to be calculated by 2's complement. The position register is saved to the buffer.

(7) End: The program ends.

(8) Measurement: After the program ends, the position register saved in the buffer can be transferred to the real world displacement. The following equation describes how position is calculated from the value in the position register:

$$Position = Position\ register \times \frac{\lambda}{N} \times Compensation\ number$$

where:

$\lambda = 632.99135$ nanometers (for HP5517C)

$N = 64$ when linear optics are being used

$N = 128$ when plane mirror optics are being used

$N = 256$ when high resolution optics are being used

$$Compensation\ number = \frac{1}{Air's\ index\ of\ refraction} = 0.9997288$$

Then the experimental results will be plotted into a time-position graph step by step continuously. These files can help us to compare the results of different driving waveforms..

4.2 Experiment Results of 1-D IDM Model

The forward movement of one-dimension IDM is similar to the backward movement but little difference in step size. With same condition but converse duty, the step of the backward movement is larger than that of the forward movement. One possibility is to assume the friction between the bottom of one-dimension IDM and the surface of the guide in forward and backward is quite different since the inaccurate manufacture of IDM. Another possibility may be the sudden stop of the principles of one-dimension IDM illustrated in Figure 2.1. The difference between forward and backward movement results from the sudden stop of the counter-mass which contributes to the displacement in the same direction or not. Because of the difference between the forward and backward movement of the one-dimension IDM, we should know the degree of the difference. Base on the condition of manufacture, two piezoelectric actuators applied the same voltage waveform cannot produce the same movement.

4.3 Experimental Setup of 2-D IDM Model

The most parts of the experiment setup are the same. The only difference is the measuring system is that the laser interferometer is replaced by digital camera. The procedures of the experiment of 2-D IDM are listed below.

(1) DSP module send asymmetric triangular input waveforms to the amplifier.

(2) The inputs are amplified and sent to the piezoelectric actuators then.

(3) It will get the image data by camera.

After we get the image, the data will be processed to calculate the movement of the 2-D IDM, like translation and rotation. Figure 4.9 and Figure 4.10 are the picture of the setup about the system used to obtain the image data.

4.4 Experiment Results of 2-D IDM Model

Figure and Figure are two different pictures. First is in zero second and second is in thirty second. The area of grid in the picture is one square centimeter. Figure and Figure are the same as before two pictures. The degree between line by line is ten degree. The first experiment is to make the 2-D IDM move up linearly and no rotation occurs by using upper two piezoelectric actuators. The results are shown as Figure 4.11 to Figure 4.12. The results of first just like what we expect. The 2-D IDM just moved up linearly and there is no rotation. The pictures from Figure 4.13 to Figure 4.14 are the results of second experiment. The movement of IDM in second experiment is the same as in first experiment. But these results are not so desired. The IDM moved not only up but also right. The magnitude of upward movement is twice of rightward movement. The pictures from Figure 4.15 to Figure 4.16 are the results of third experiment. The movement that we expect is pure rotation by using three

actuators. These results are not desired also. The IDM moved downward and leftward when the rotation occurred. The 2-D IDM moved 0.3 μm upward per step in first experiment. In second experiment the IDM moved 0.2 μm rightward and 0.44 μm upward each step. In third experiment the IDM moved 0.17 μm rightward, 0.11 μm downward each step and was rotated about 5.56×10^{-4} degree each step. Based on the comparison of the result of simulations and experiment, prediction about translation of 2-D IDM is more accurate than rotation.

Chapter 5 Conclusion

In this research, we found that the 2-D IDM can be realized to achieve the purpose of precise positioning. According to the results of simulations and experiments, the movement of 2-D IDM can be controlled by us and it can be predicted. It help us to develop this mechanism for precise positioning. Here we have some conclusion as below.

(1)　The applied voltage increases, the IDM will move and rotate faster.

(2)　Because of the difference of forward and backward movement, it needs to adjust the applied voltage to obtain the same movement.

(3)　There are six directions we can control the 2-D IDM to move directly only by using two actuators.

(4)　The bigger the phase lag between three input waveforms be, the slower 2-D IDM rotate.

There are still some problem in this experiment included how to estimate the parameters of system, the frictional coefficient especially. The other problem is the cable of the actuator. When the IDM is moving, the cable which get stuck produce force to push or pull the mechanism. The only way to solve this problem is to reduce the radius of the cable. It can reduce the weight and affection of the cable. Measure is the most important problem because the pixels of digital camera are limited. This measuring system cannot help us to obtain more accurate data. It needs more accurate image process system to obtain image data and to calculate the movement of the 2-D IDM. There is one problem occurred. The

contact between the plate and the surface is not close, especially in the center of the plate.

The 2-D IDM will be developed to be more accurate and reliable by solving the above problems in the future.

Reference

[1] S. Ling, H. Du & T. Jiang, "Analytical and Experimental Study on a Piezoelectric Linear Motor", *Smart Materials and Structures*, Vol.7, No.3, Jun, 1998, pp.382-388.

[2] T. Higuchi, Y. Yamagata, K. Furutani & K. Kudoh, "Precise Positioning Mechanism Utilizing Rapid Deformations of Piezoelectric Elements", *Proceedings of the IEEE MEMS Workshop*, 1990, pp.222-226.

[3] J. Mendes, M. Nishimura, K. Tomizawa, Y. Yamagata & T. Higuchi, "Print Board Positioning System Using Impact Drive Mechanism", *Proceedings of the SICE Annual Conference*, Jul, 1996, Tottori, Jpn, pp.1123-1128.

[4] K. Furutani, T. Higuchi, Y. Yamagata & N. Mohri, "Effect of Lubrication on Impact Drive Mechanism", *Precision Engineering*, Vol.22, No.2, 1998, pp.78-86.

[5] M. Kurisu, T. Yoshikawa, "Tracking Control for An Object in Pushing Operation", *Proceedings of the 1996 IEEE/RSJ International Conference on Intelligent Robots and Systems*, Vol.2, Nov, 1996, Osaka, Jpn, pp.729-736.

[6] Y. Wang, M. Mason, "Two-Dimensional Rigid-Body Collisions with Dry Friction", *Transactions of the ASME*, Vol.59, Sep, 1992, pp.635-642.

[7] Y. Yamagata, T. Higuchi, "A Micropositioning Device for Precision Automatic Assembly Using Impact Force of Piezoelectric Elements", *Proceedings of IEEE International Conference on Robotics and*

Automation, May, 1995, Nagoya, Jpn, pp.666-671.

[8] H. Alexander, H. Lakhani, "Robotic Control of Sliding Object Motion and Orientation", *Proceedings of the 1996 IEEE/RSJ International Conference on Robotic and Automation*, Apr, 1996, Minneapolis, Minnesota, pp.3336-3342.

[9] K. Furutani, N. Mohri & T. Higuchi, "Self-Running Type Electrical Discharge Machine Using Impact Drive Mechanism", *Proceedings of IEEE/ASME International Conference on Advanced Intelligent Mechatronics*, Jun, 1997, Tokyo, Jpn, pp.88.

[10] K. Furutani, N. Mohri & T. Higuchi, "Self-Running Type Electrical Discharge Machine Using Impact Drive Mechanism", *Seimitsu Kogaku Kaishi/Journal of the Japan Society for Precision Engineering*, Vol.63, No.9, Sep, 1997, pp.1290-1294.

[11] K. Ikuta, S. Aritomi & T. Kabashima, "Tiny Silent Linear Cybernetic Actuator Driven by Piezoelectric Device with Electromagnetic Clamp", *Proceedings of the IEEE Micro Electro Mechanical Systems Workshop*, Feb, 1992, Travemuende, Ger, pp.232-237.

[12] T. Idogaki, H. Kanayama, N. Ohya, H. Suzuki & T. Hattori, "Characteristics of the Piezoelectric Locomotive Mechanism for an In-Pipe Micro Inspection Machine", *Proceeding of the International Symposium on Micro Machine and Human Science*, Oct, 1995, Nagoya, Jpn, pp.193-198.

[13] 鄭仲哲,「利用壓電致動器之精密定位」,國立交通大學,博士論文,民國 92 年。

[14] 陳立明,「微步進機構定位之研究」,國立交通大學,碩士論文,

民國 94 年。

[15] 林容益，<u>DSP/CPLD 控制技術及應用</u>，初版，全華出版社，台北，

民國 90 年。

[16] 新華電腦，<u>DSP 從此輕鬆跑（TI DSP 320LF2407A）</u>，初版，台科

大圖書股份有限公司，台北，民國 92 年。

$$\text{scanning device}\begin{cases}\text{mechanical amplified}\begin{cases}\text{linear}\\\\\text{rotational}\end{cases}\begin{cases}\text{simple levered}\\\text{paralle log ram levered}\\\text{others}\end{cases}\\\\\text{direct driven}\begin{cases}\text{linear}\\\\\\\text{rotational}\end{cases}\begin{cases}\text{linear}\\\text{bending}\\\text{torsional}\\\text{shearing}\end{cases}\end{cases}$$

$$\text{pulse drive}\begin{cases}\text{stick}-\text{slip device}\begin{cases}\text{linear}\\\\\text{rotational}\end{cases}\begin{cases}\text{impact drive mechanism}\\\\\text{piezo}-\text{wal ker}\end{cases}\begin{cases}\text{base driven}\\\\\text{slider driven}\end{cases}\\\\\text{clamping mechanism}\begin{cases}\text{linear}\\\\\text{rotational}\end{cases}\begin{cases}\text{inchworm}\\\\\text{others}\end{cases}\end{cases}$$

$$\text{ultrasonic motor}\begin{cases}\text{linear}\\\\\text{rotational}\end{cases}$$

Figure 1.1 Classification of piezoelectric positioning device
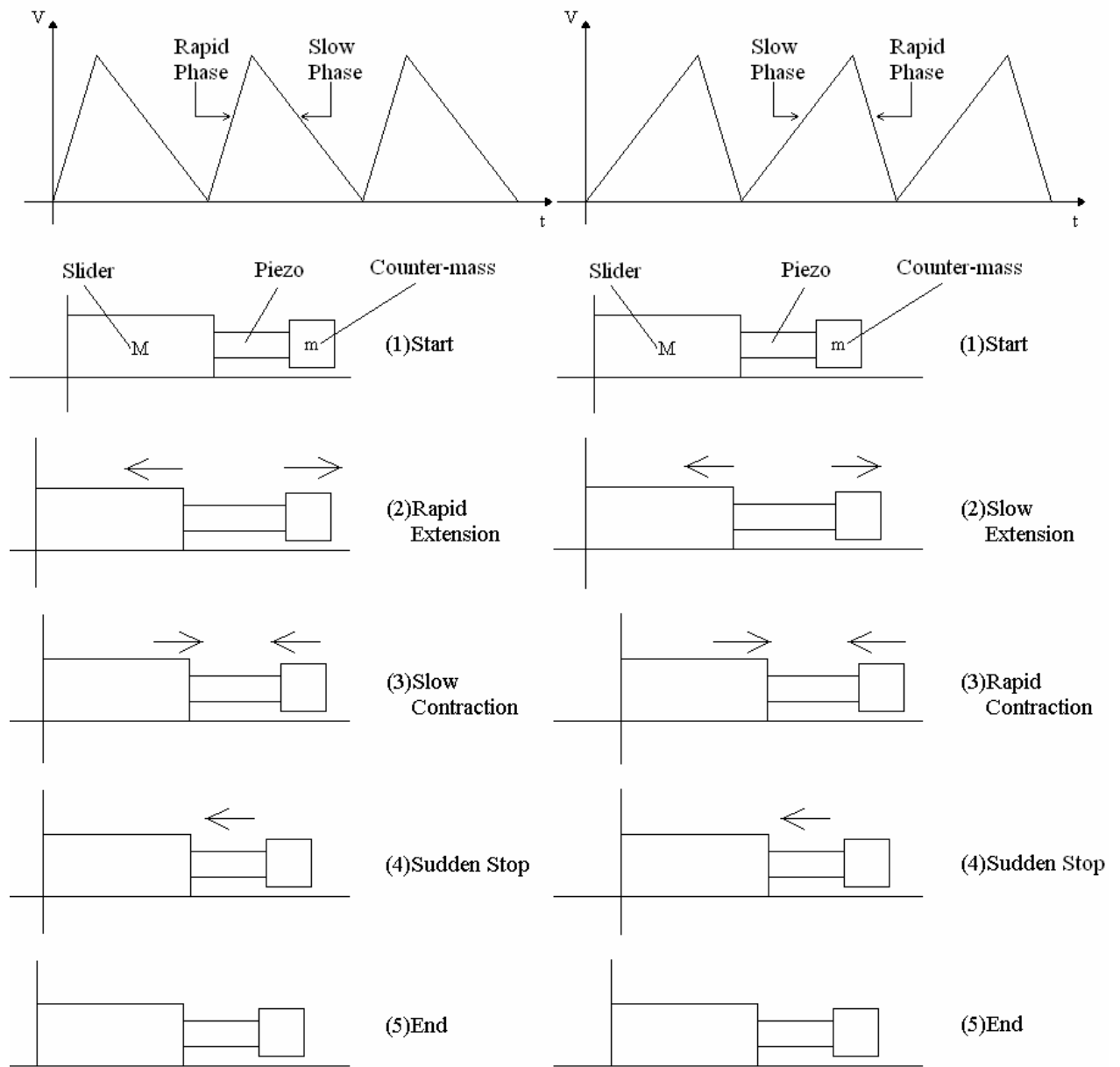
(a) backward movement   (b) input: forward

movement

Figure 2.1 Operating principle of IDM
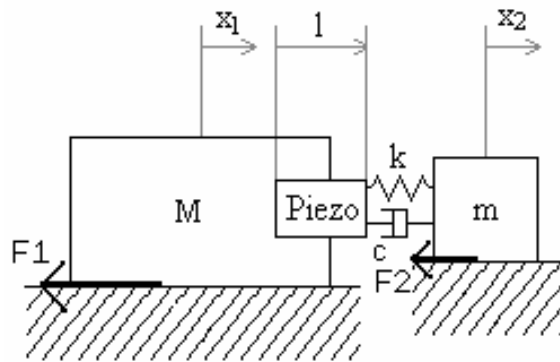
Figure 2.2 The mass-damper-spring model of 1-D IDM
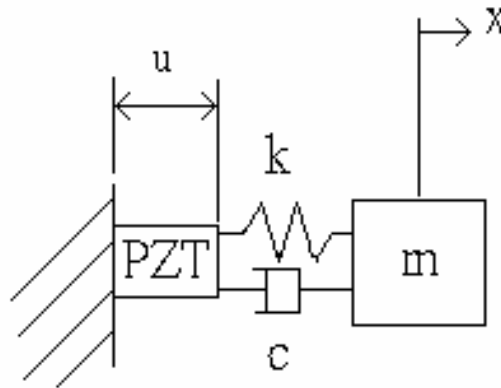
Figure 2.3 MCK model of system identification
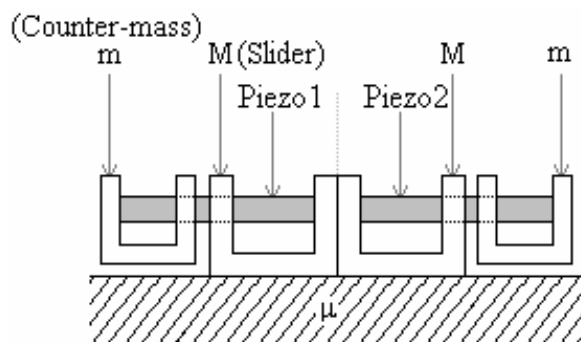
Figure 4.1 IDM structure
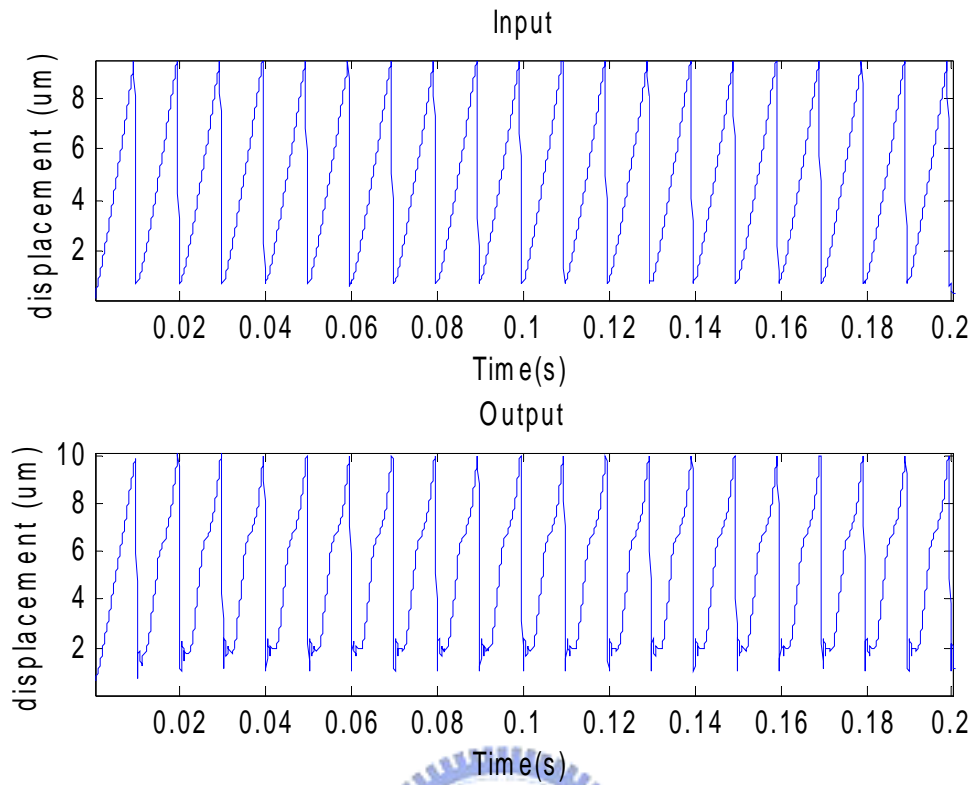
Figure 2.4 input and output of piezoelectric actuator
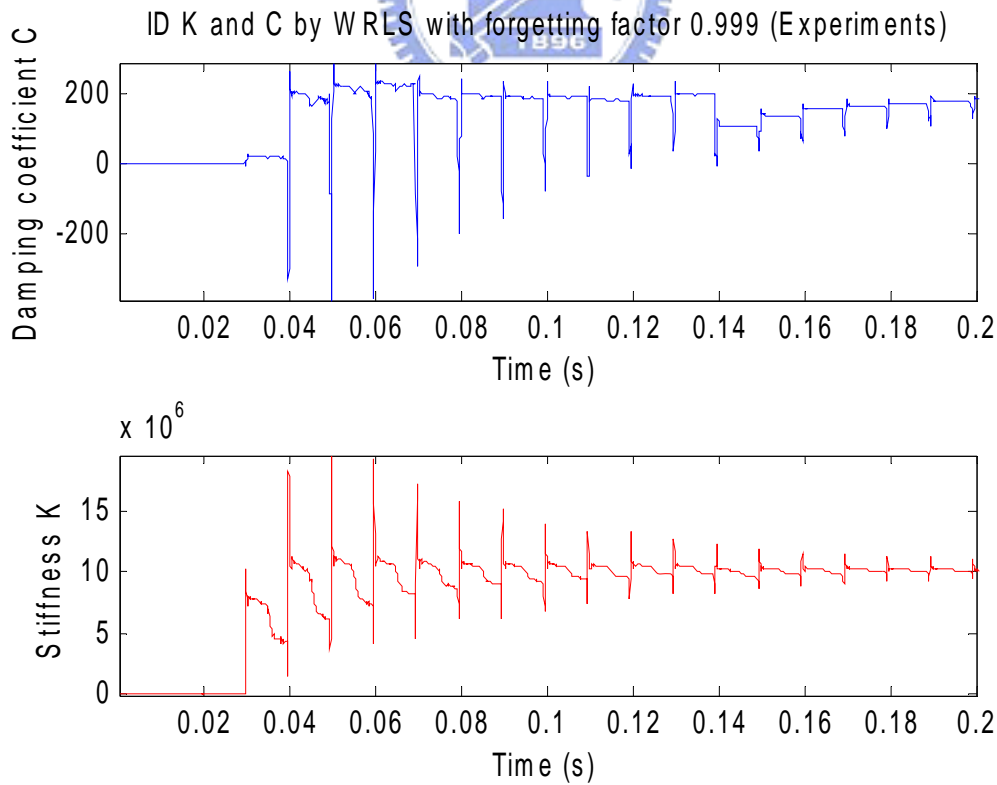
Figure 2.5 The result of estimation

35

The displacement of slider
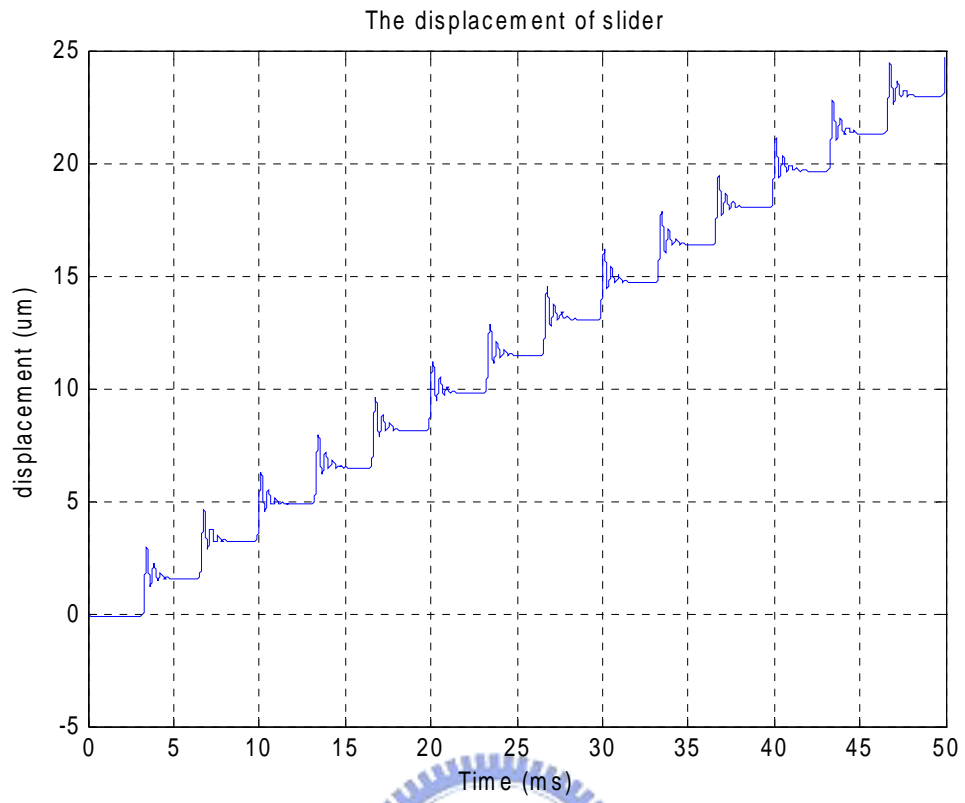
Figure 2.6 Displacement of 1-D IDM (100V, 300Hz, 95% duty)
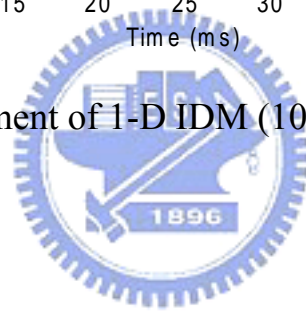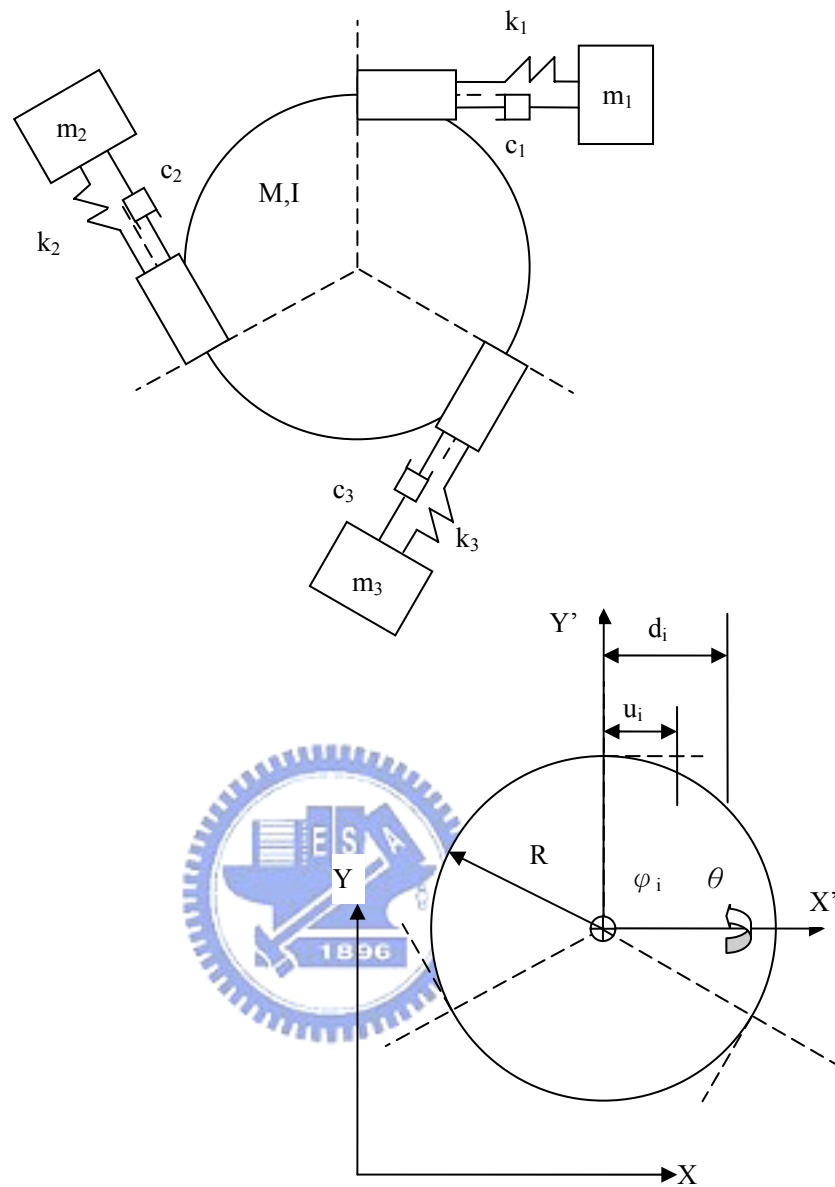
Figure 3.1 The mass-damper-spring model of 2-D IDM
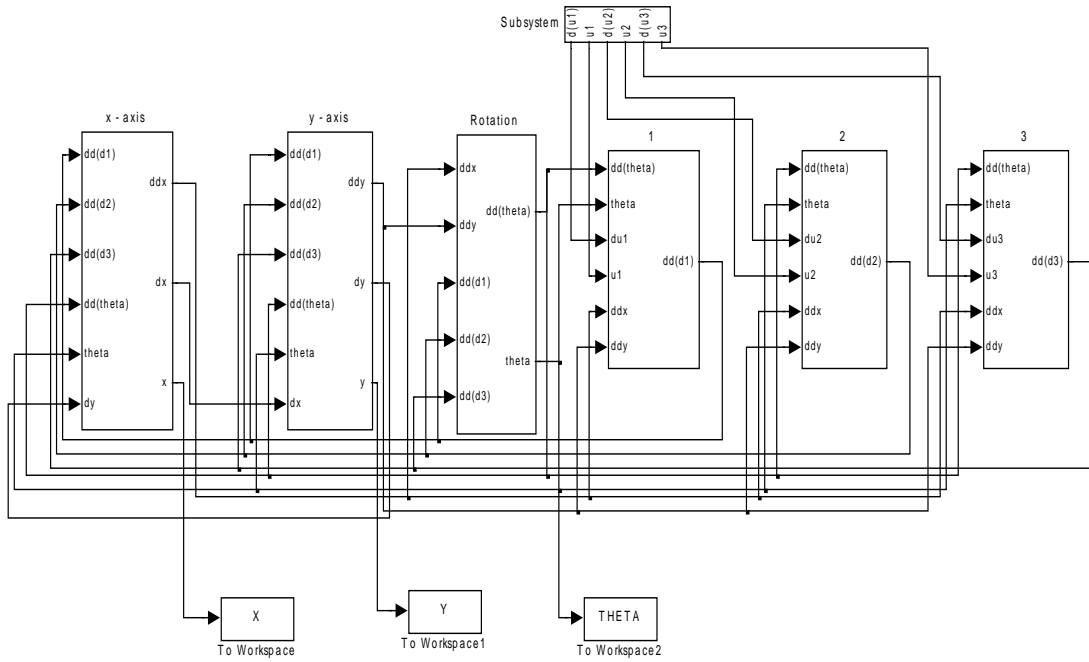
Figure 3.2 The block diagram of the model of 2-D IDM
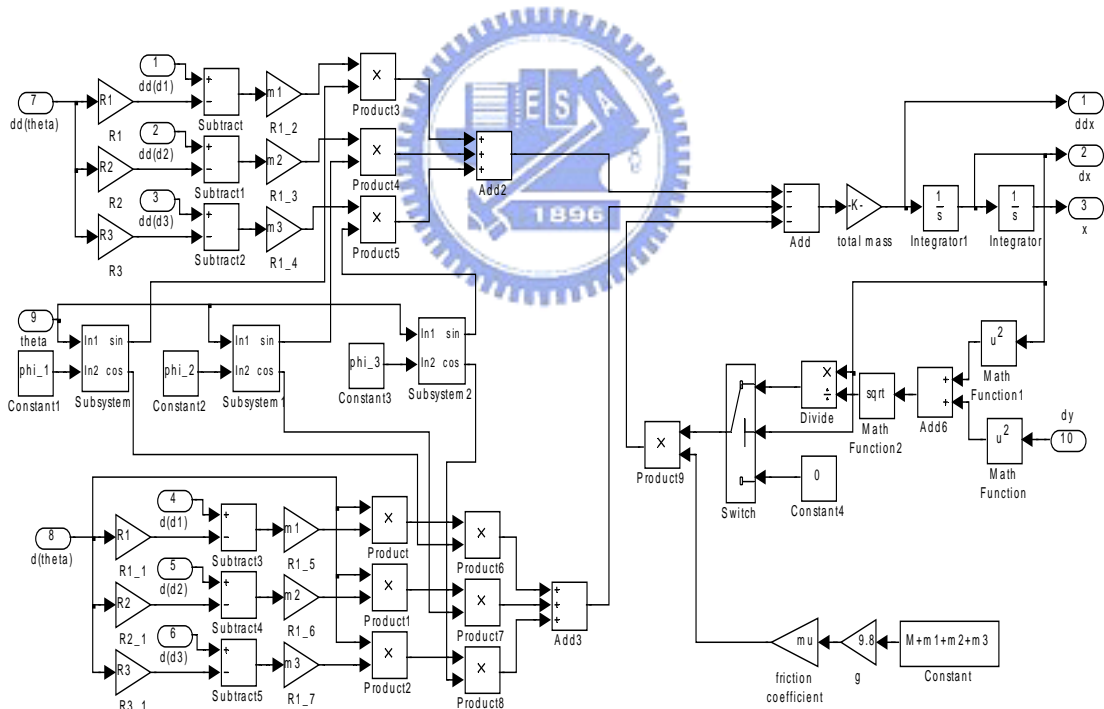
Figure 3.3 The block diagram of dynamic equation in X-axis
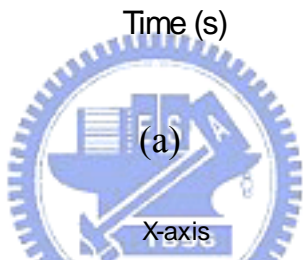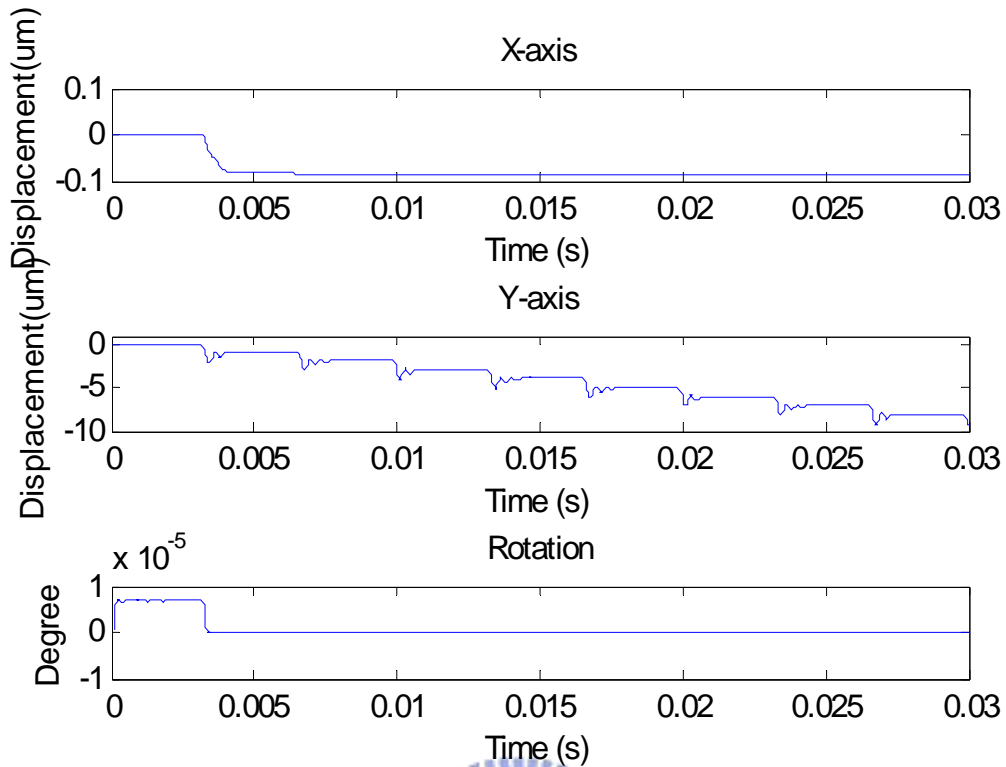
(a)
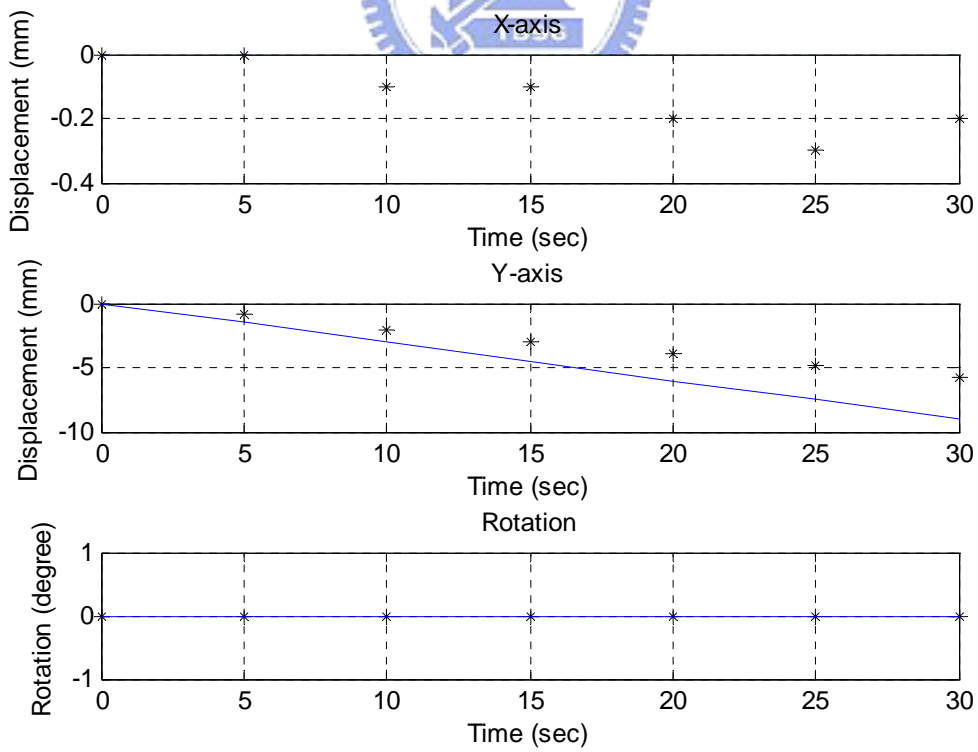
(b)

Figure 3.4 The translation in Y-axis (a) 30ms (b) 30s
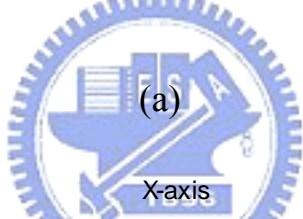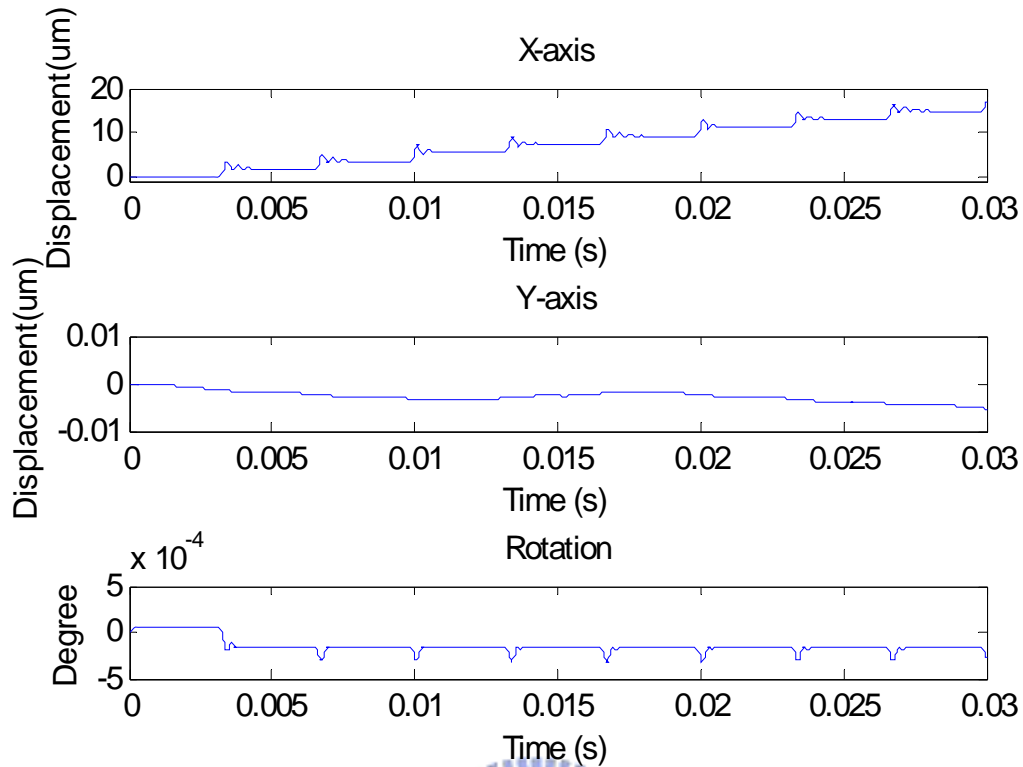
(a)
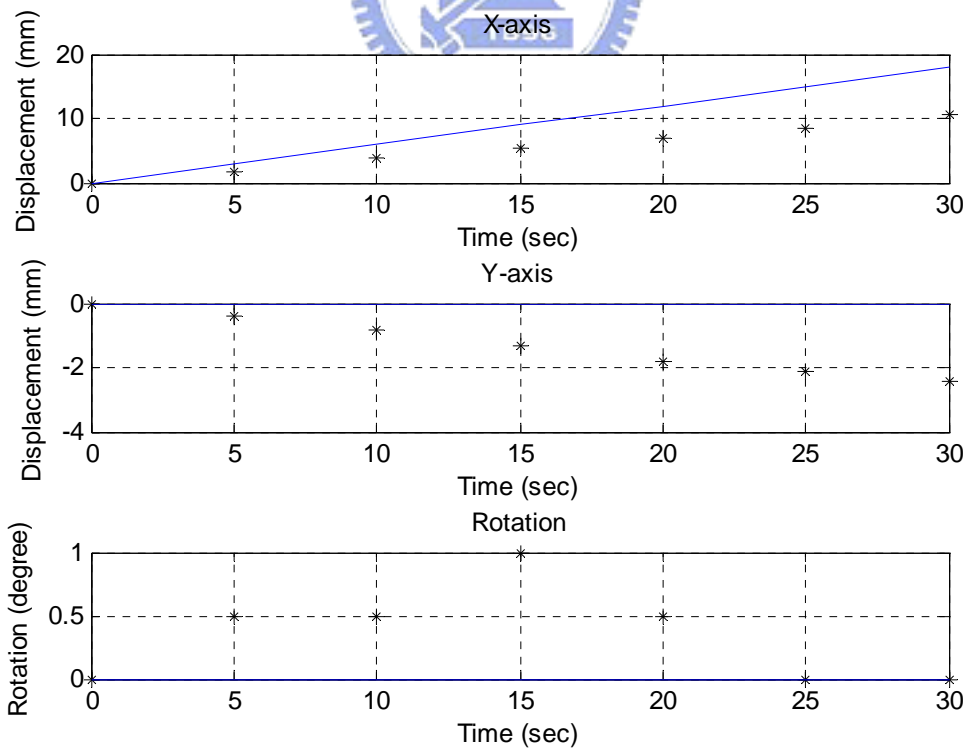
(b)

Figure 3.5 The translation in X-axis (a) 30ms (b) 30s
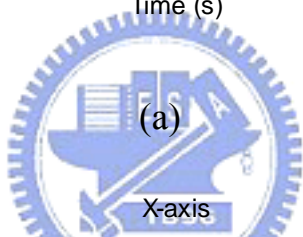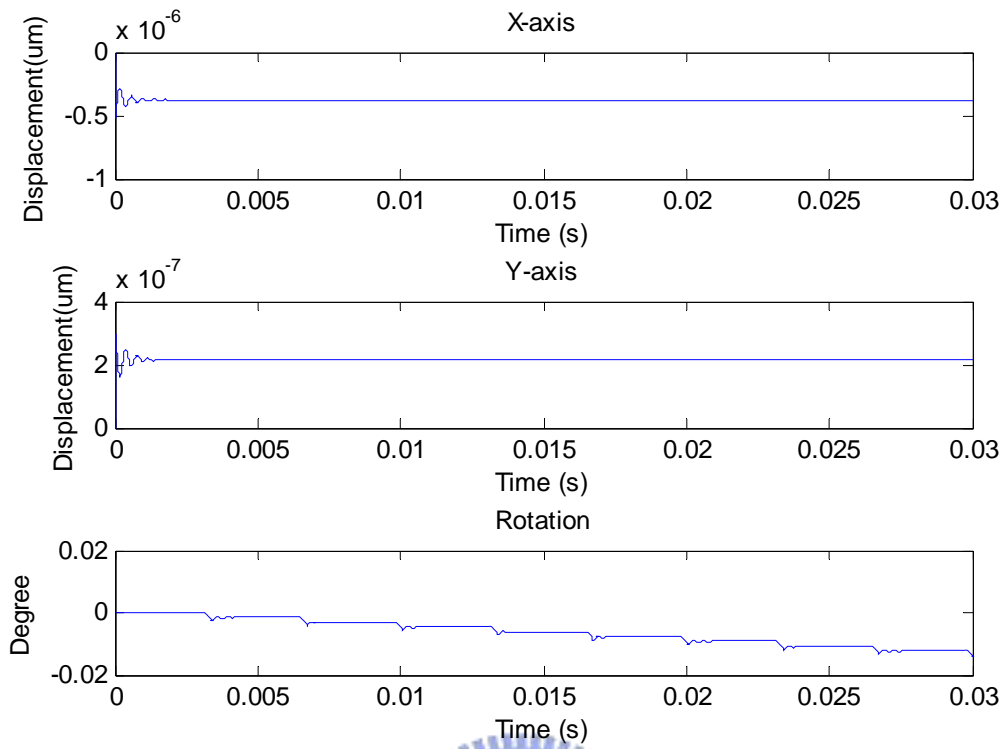
(a)
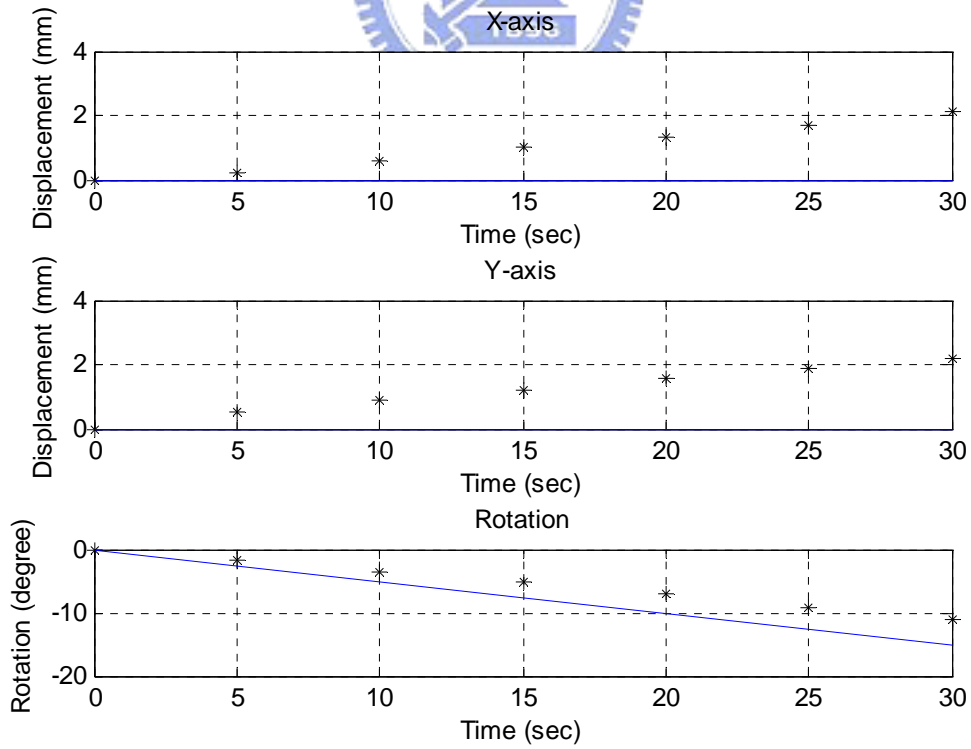
(b)

Figure 3.6 The pure rotation (a) 30ms (b) 30s
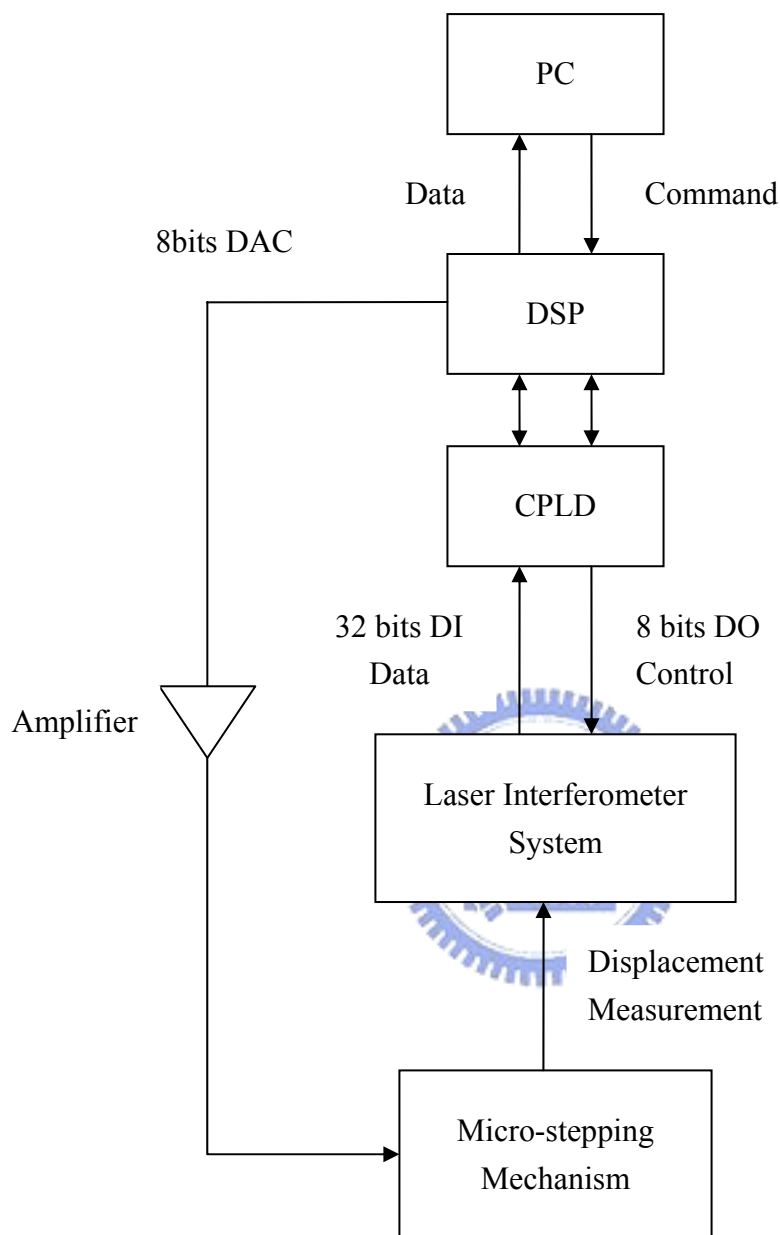
Figure 4.2 Structure for measurement for 1-D IDM
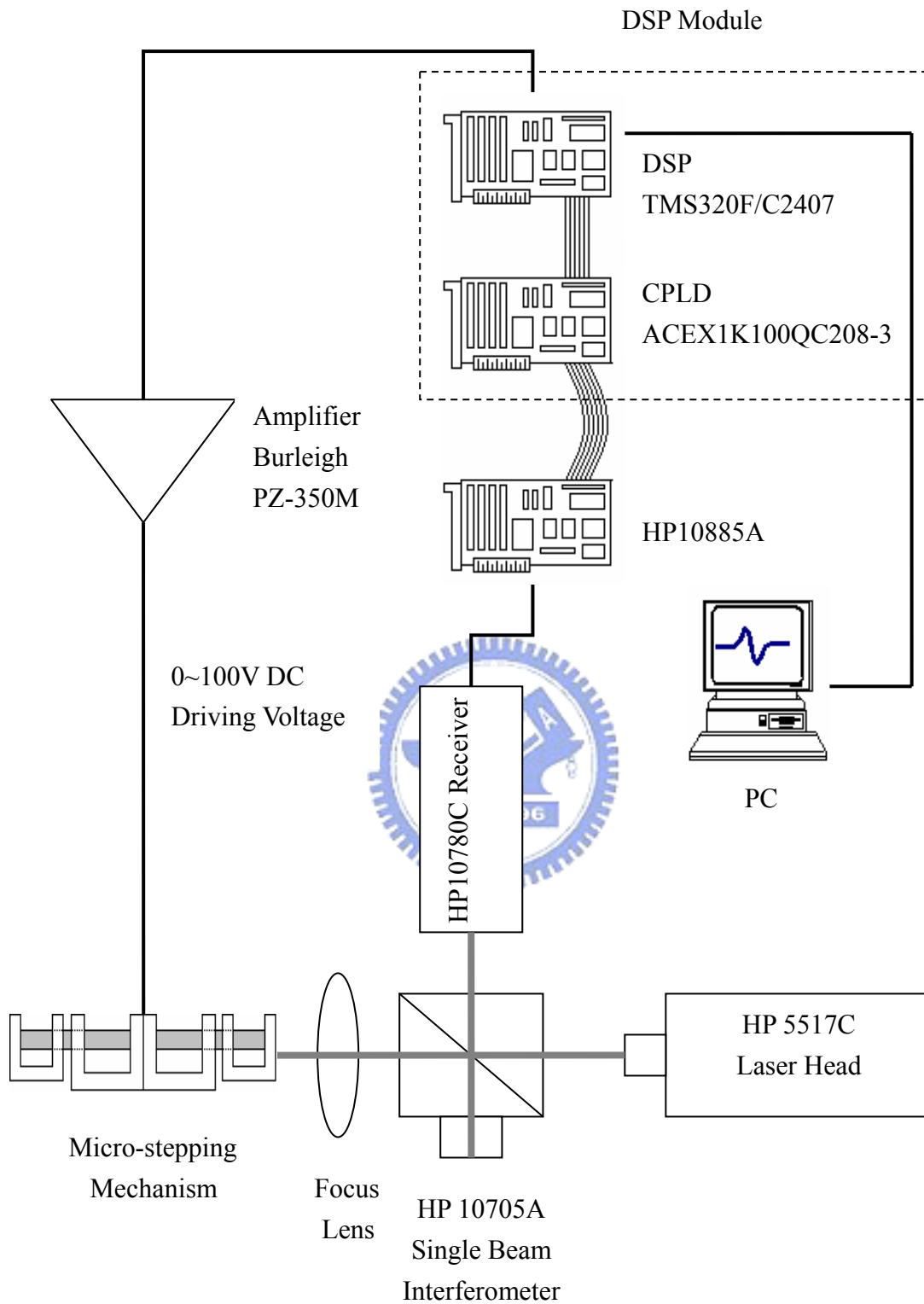
Figure 4.3 System configuration
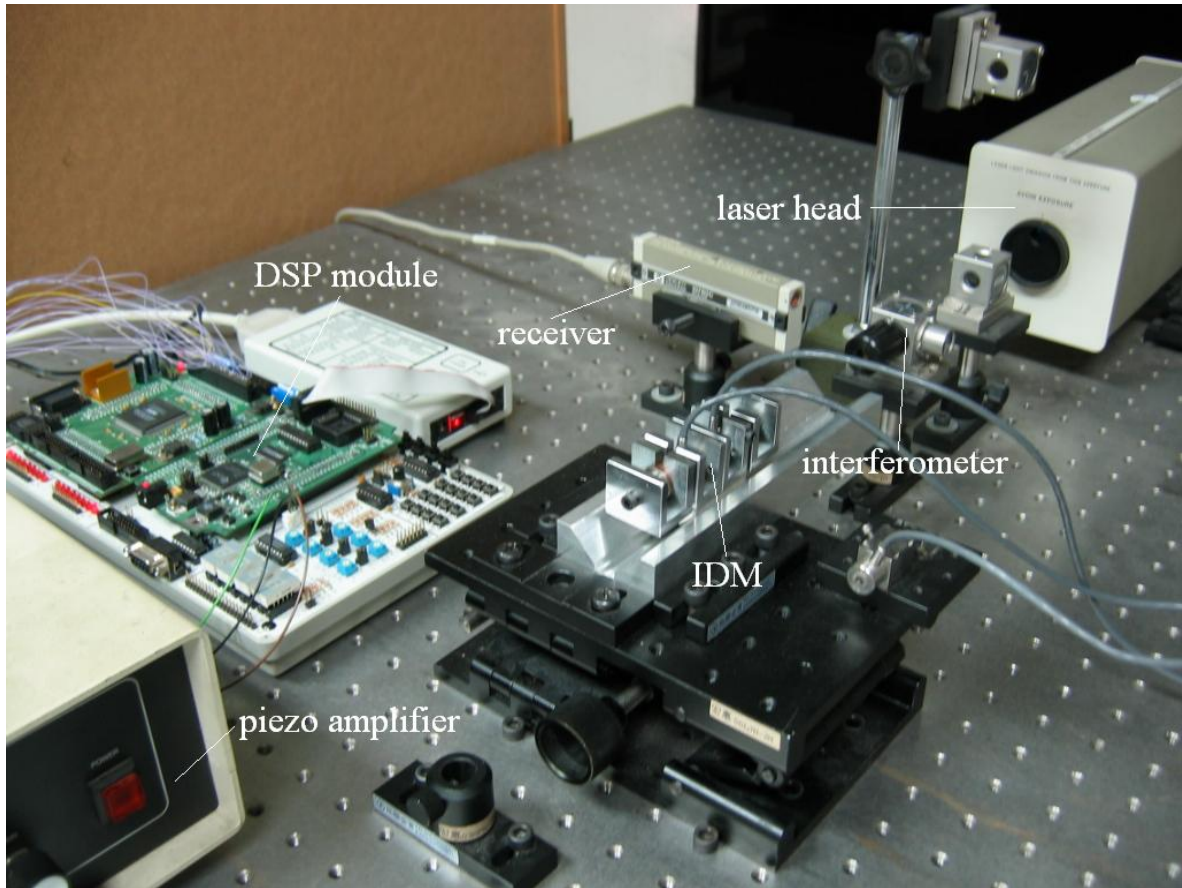
Figure 4.4 Experiment setup of 1-D IDM
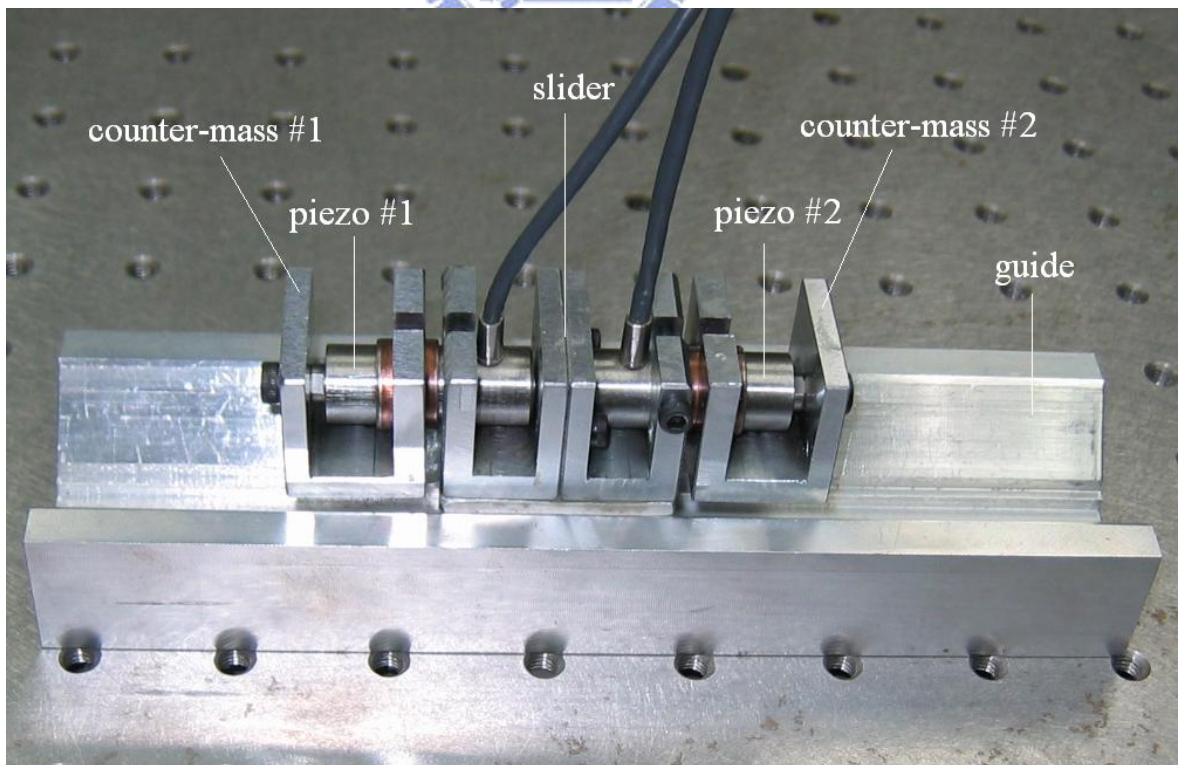
Figure 4.5 1-D Impact drive mechanism
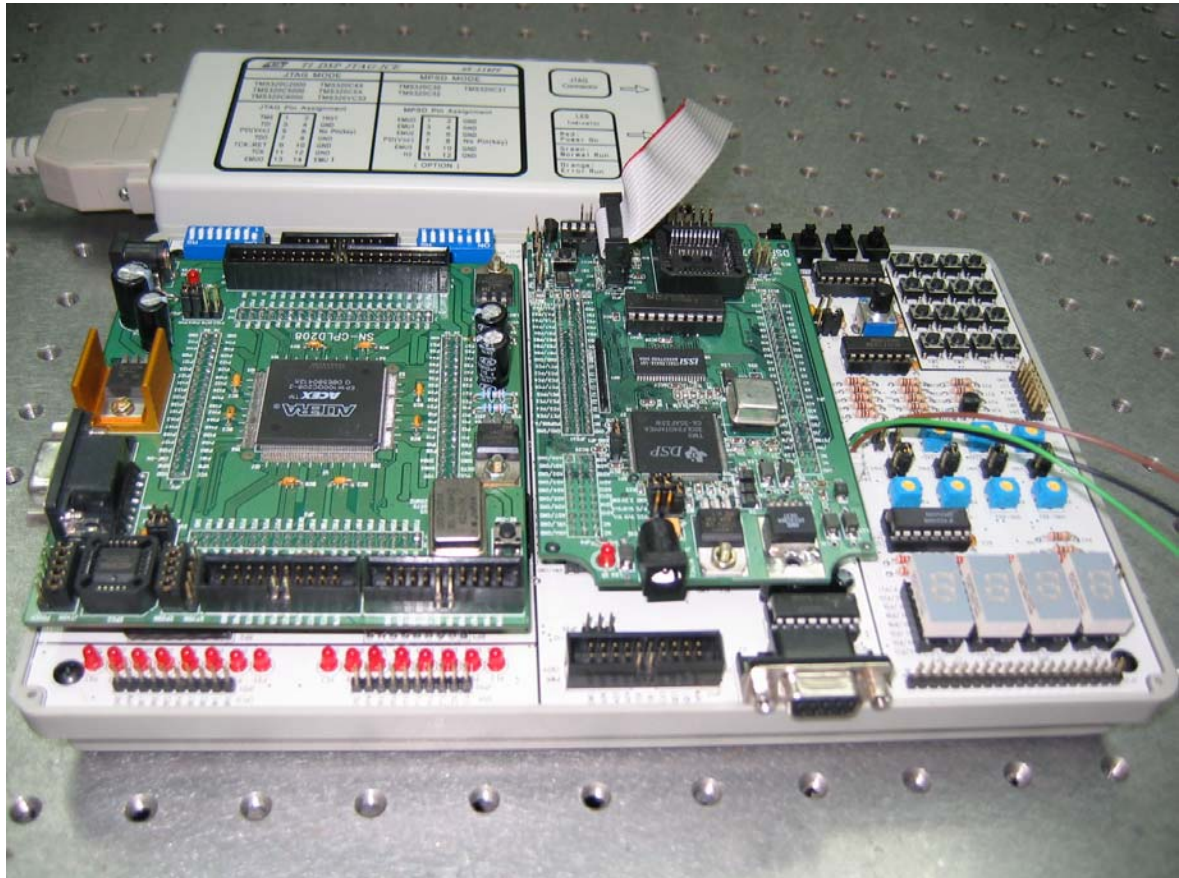
Figure 4.6 DSP module
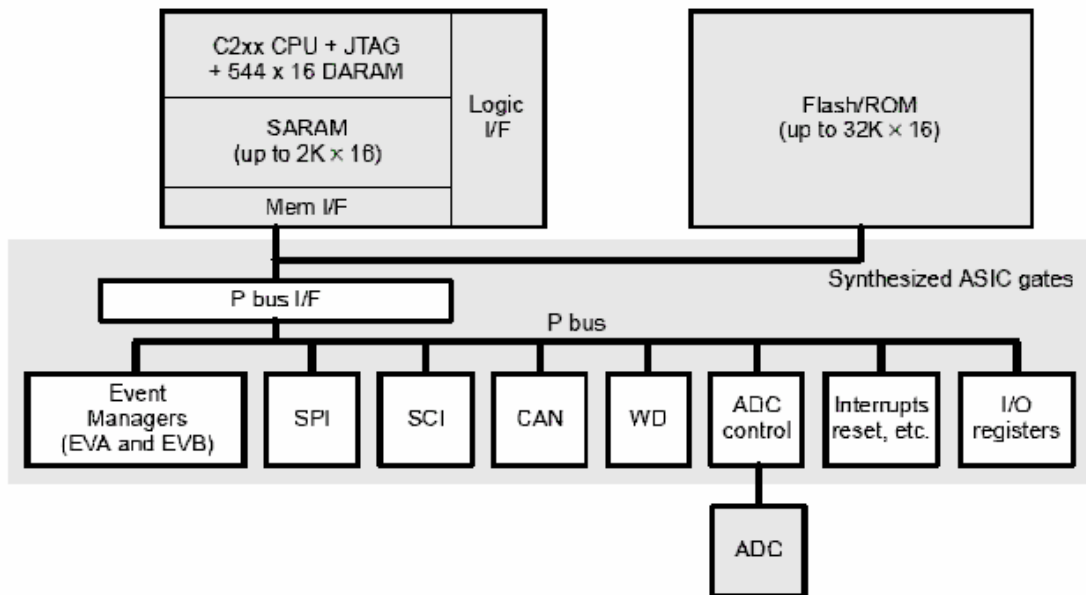
Figure 4.7 2407A device architecture
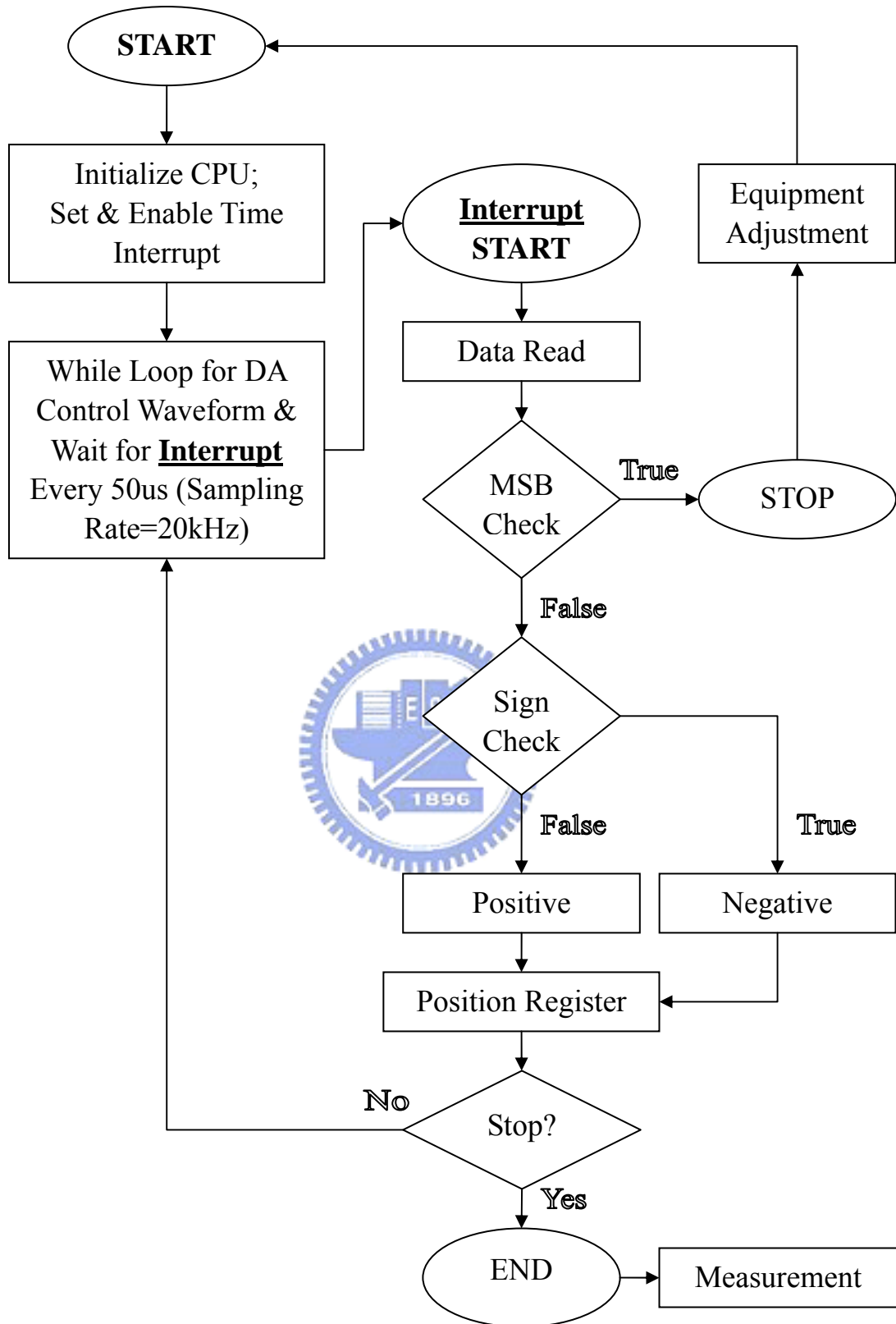
Figure 4.8 Program flow

Figure 4.9 A lateral view of measuring system
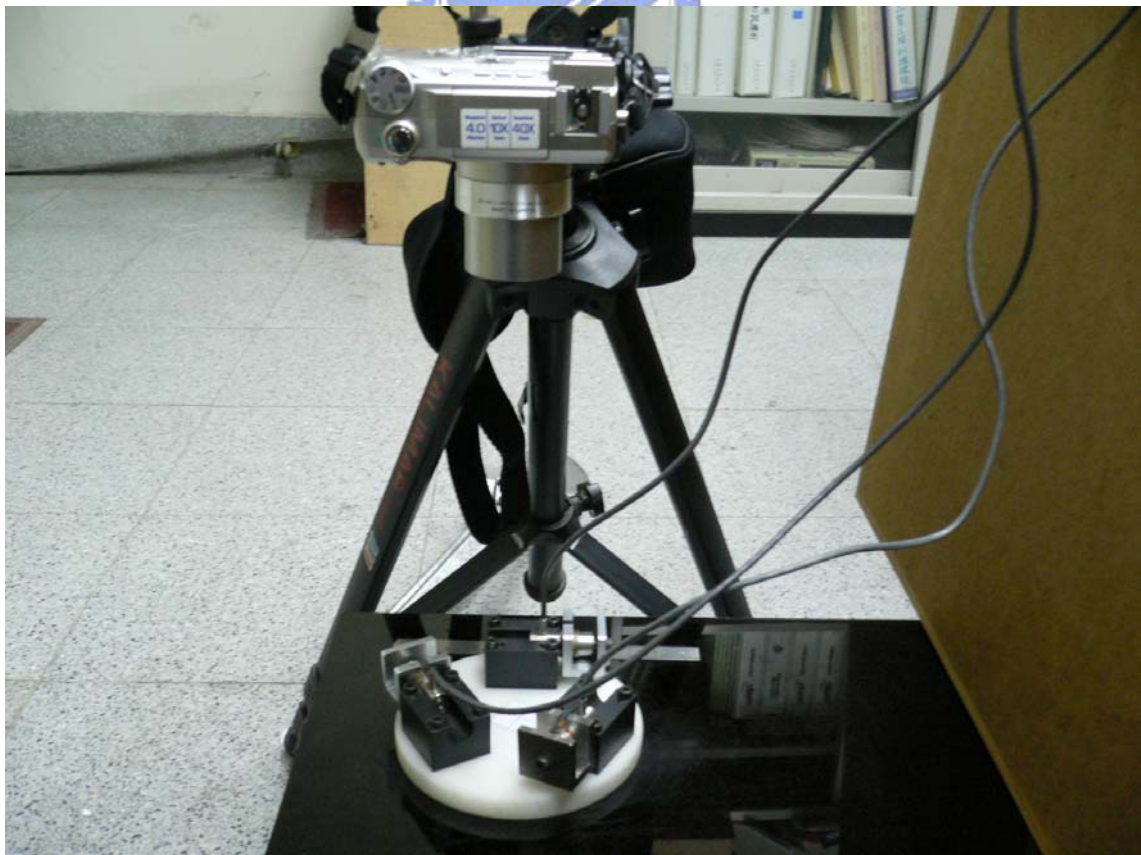
Figure 4.10 A front view of measuring system
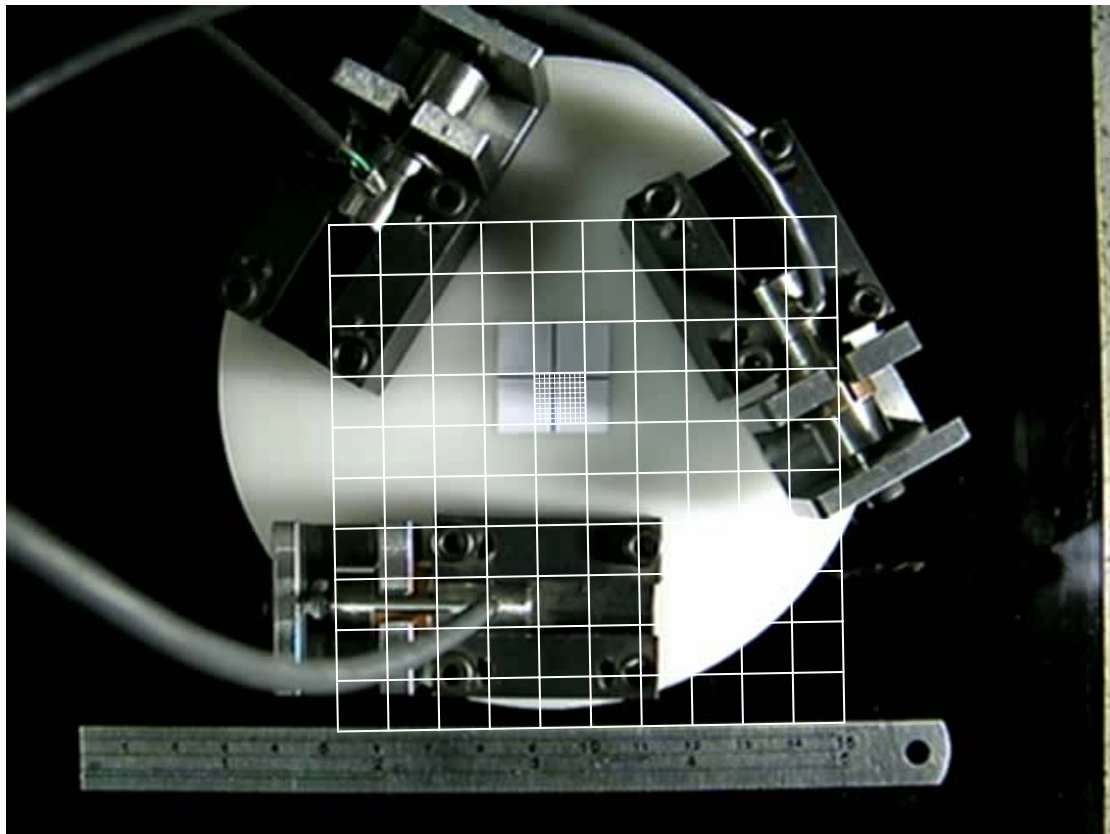
(a)
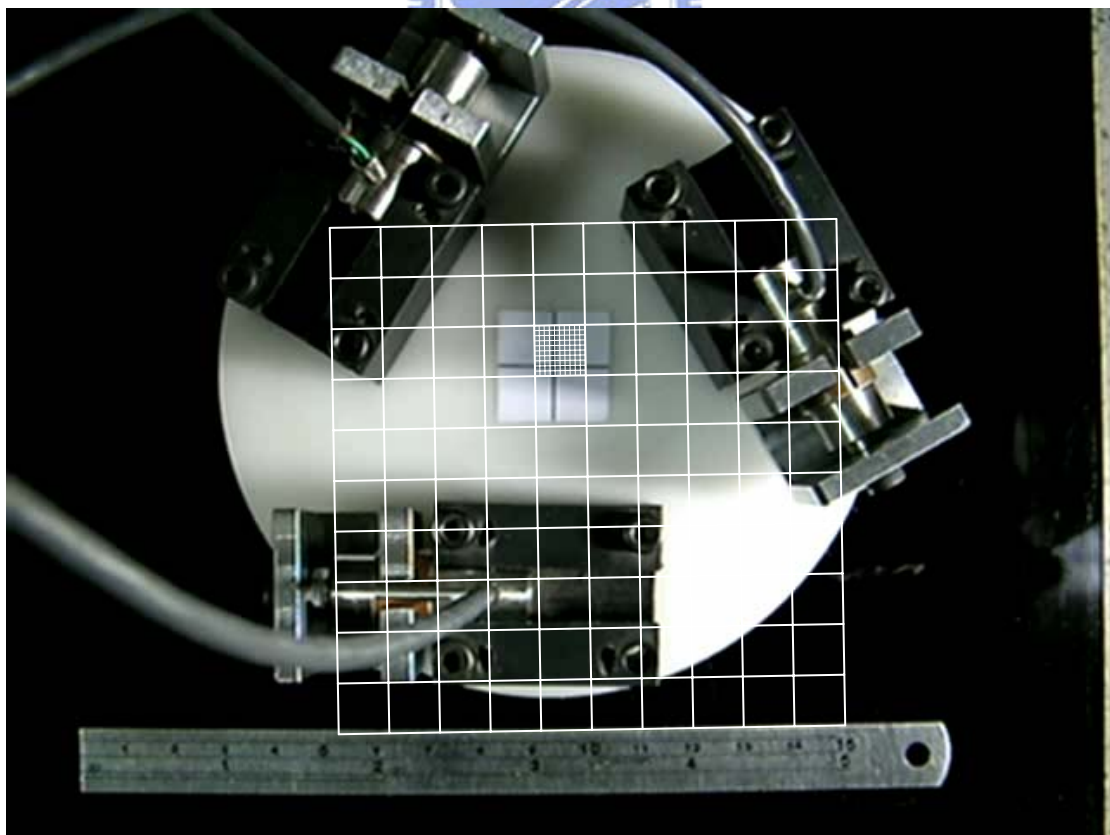
(b)

Figure 4.11 The grid diagram of 2-D IDM (first experiment) (a) 0s (b) 30s
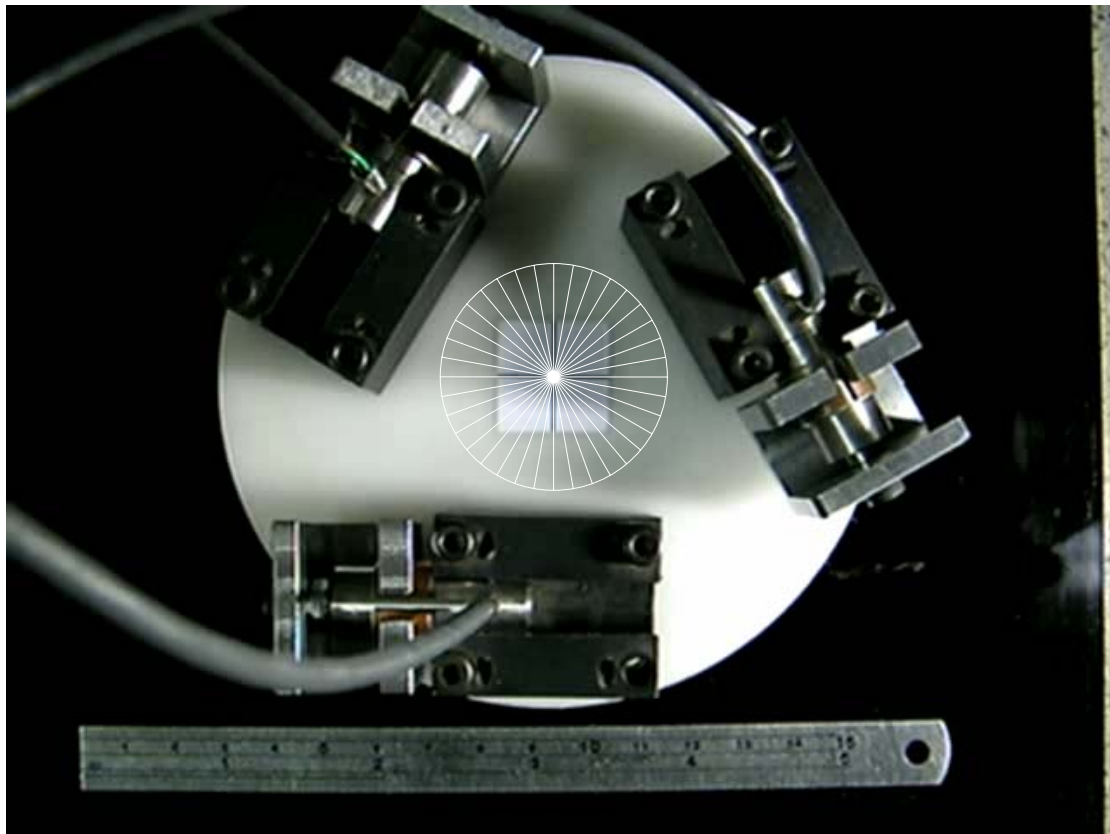
(a)
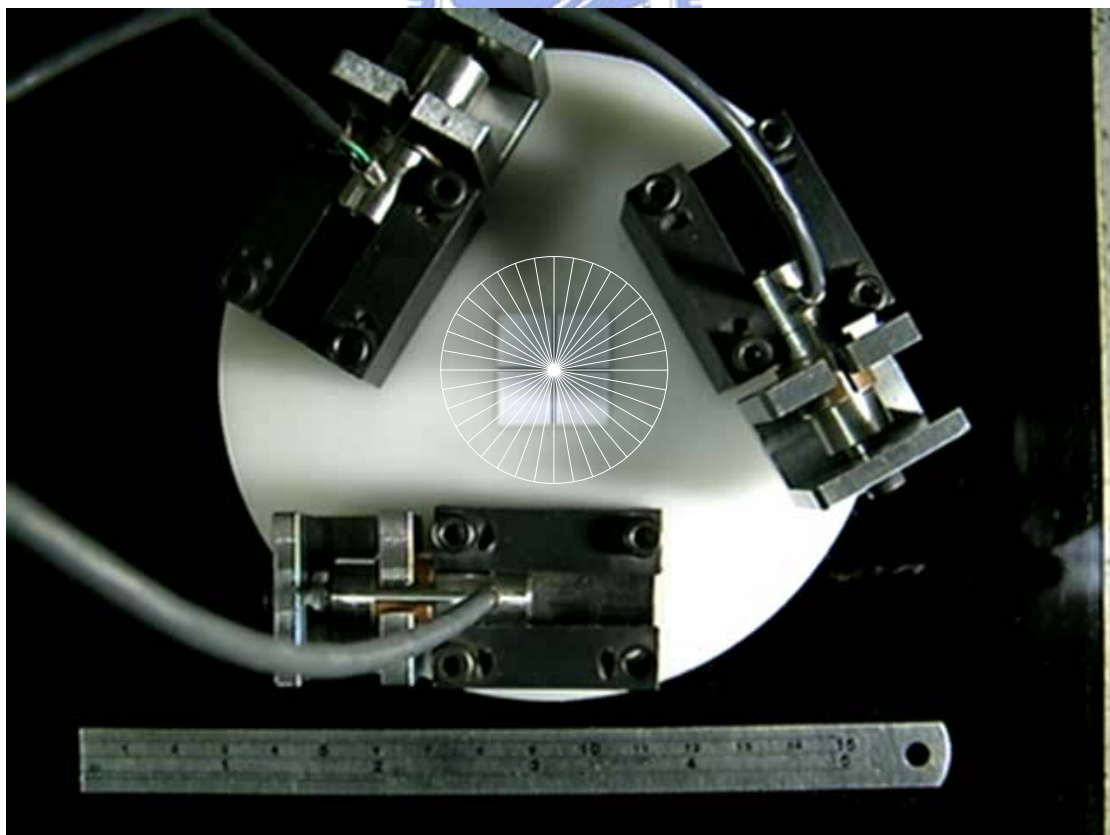
(b)

Figure 4.12 The rotate diagram of 2-D IDM (first experiment)(a)0s(b) 30s
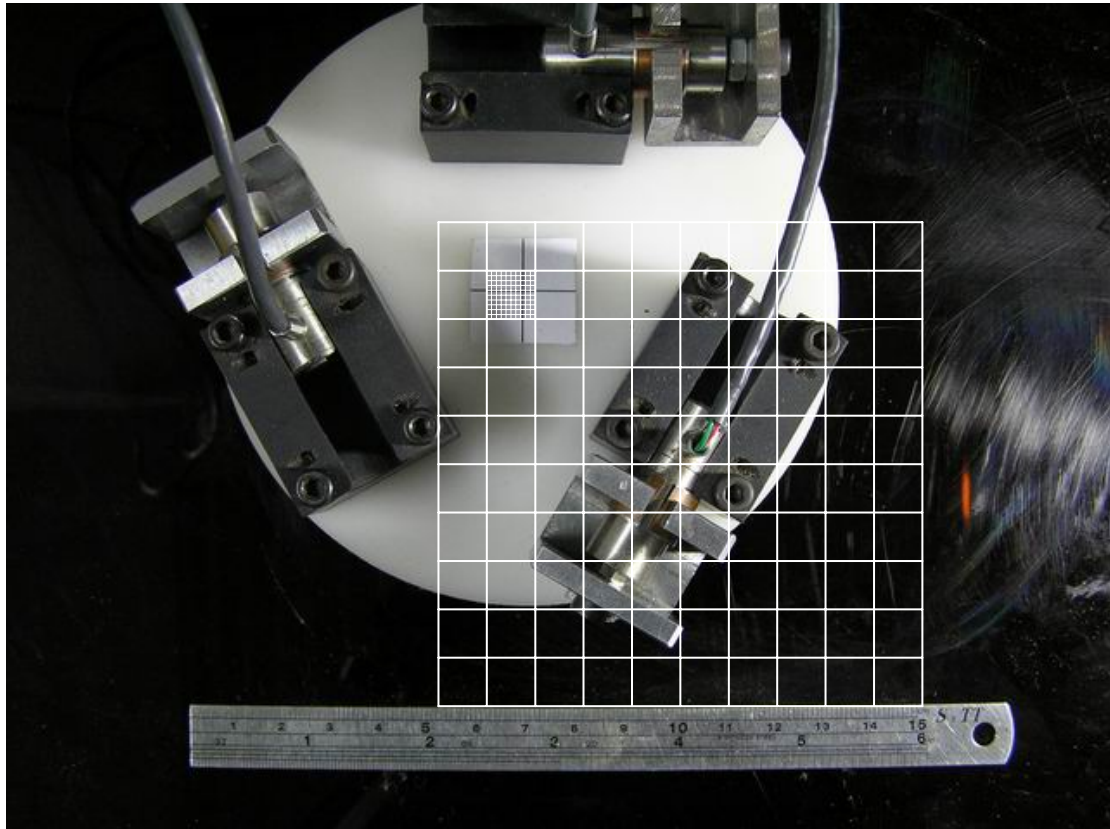
(a)
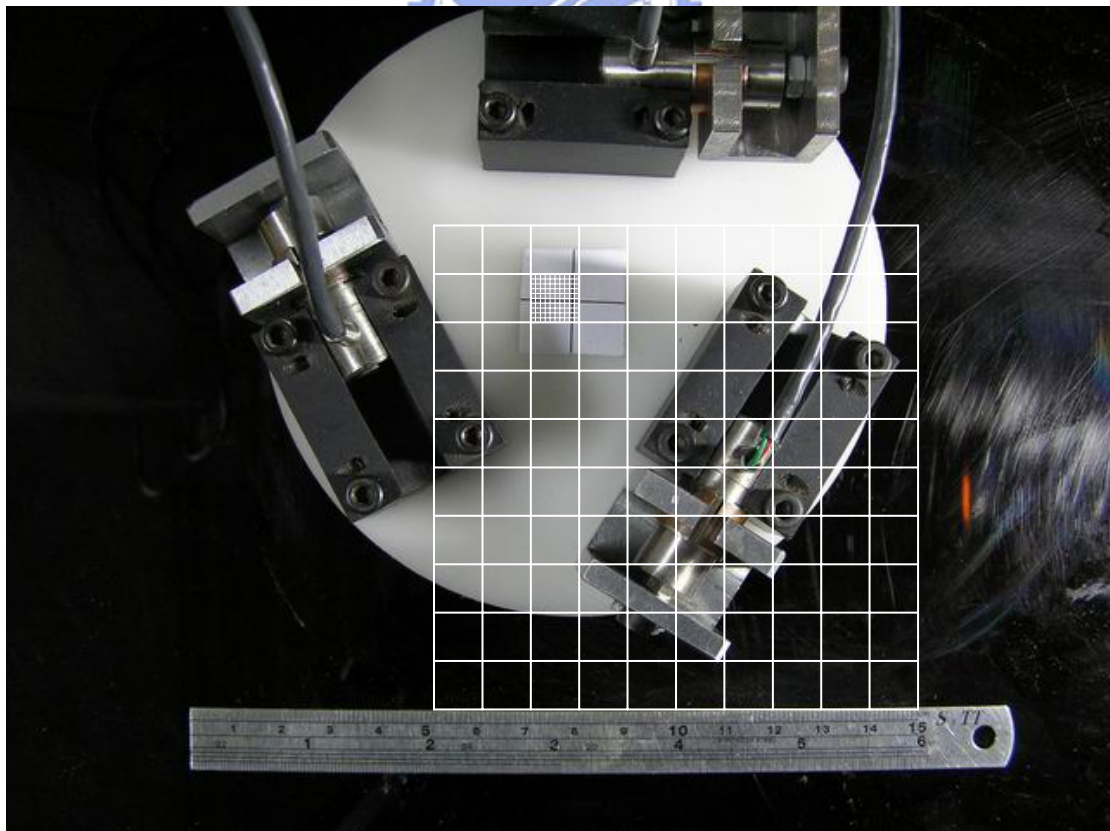
(b)

Figure 4.13 The grid diagram of 2-D IDM(second experiment)(a)0s(b)30s
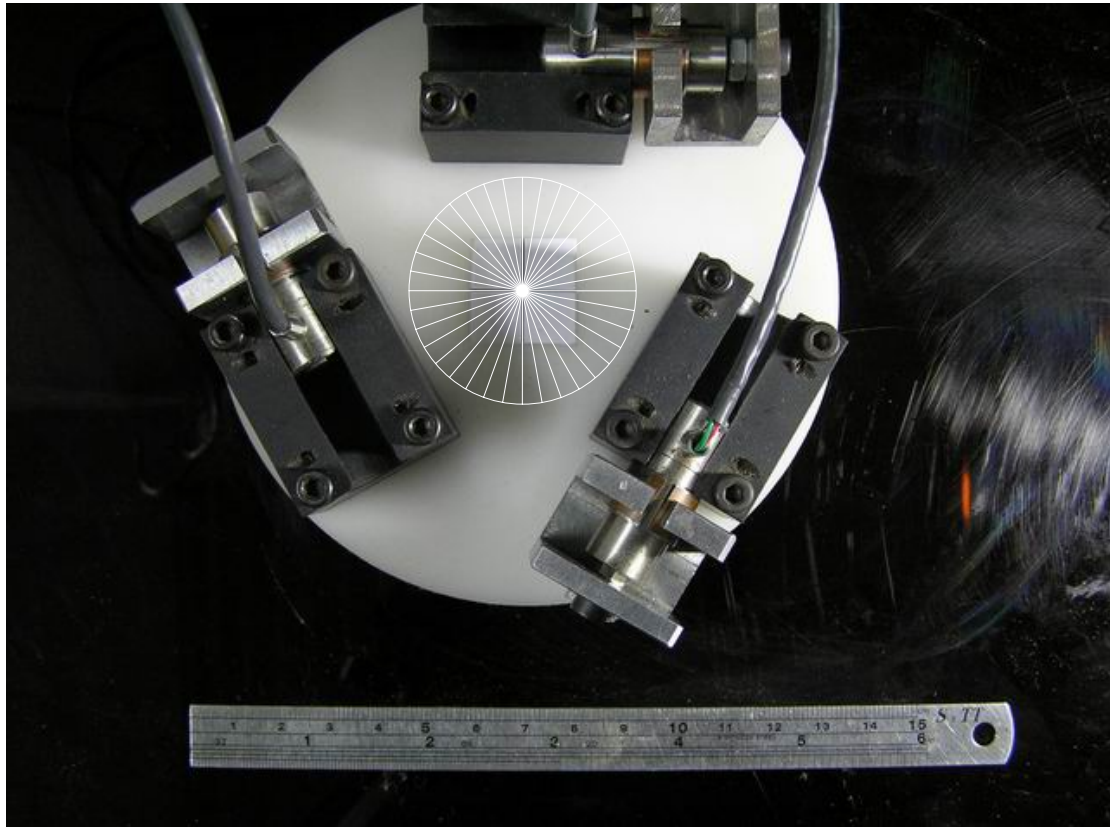
(a)
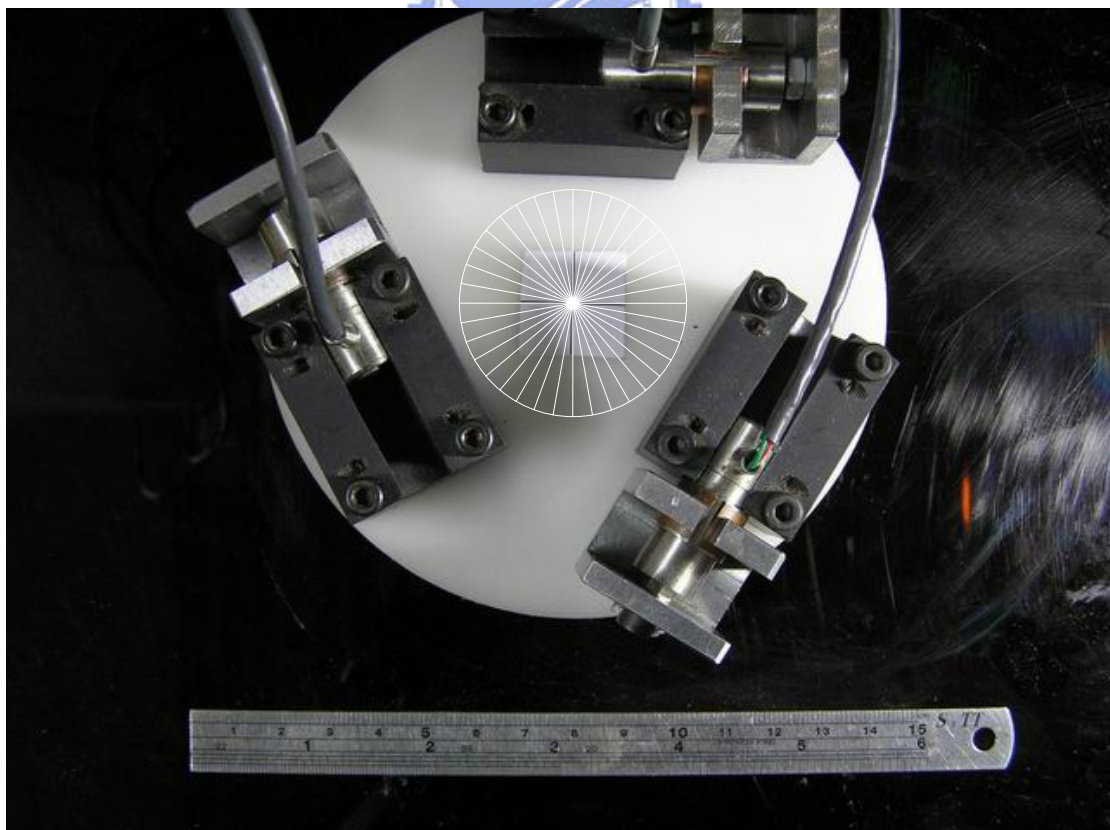
(b)

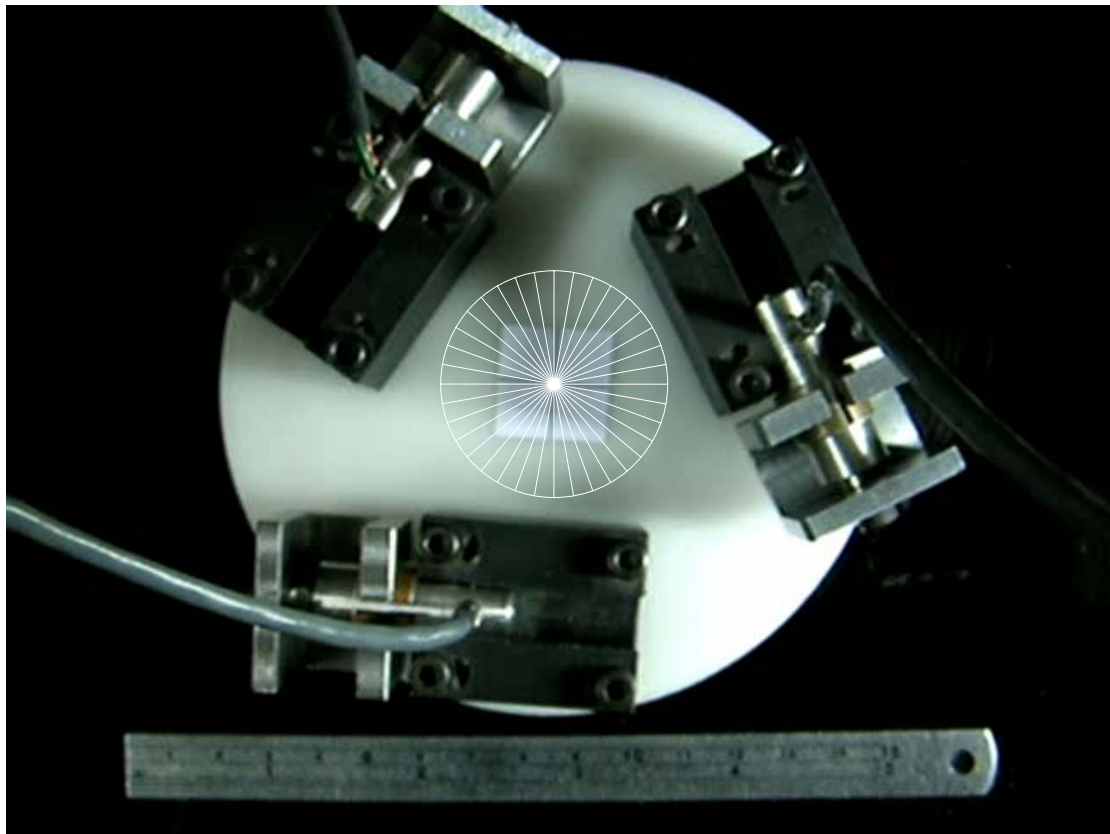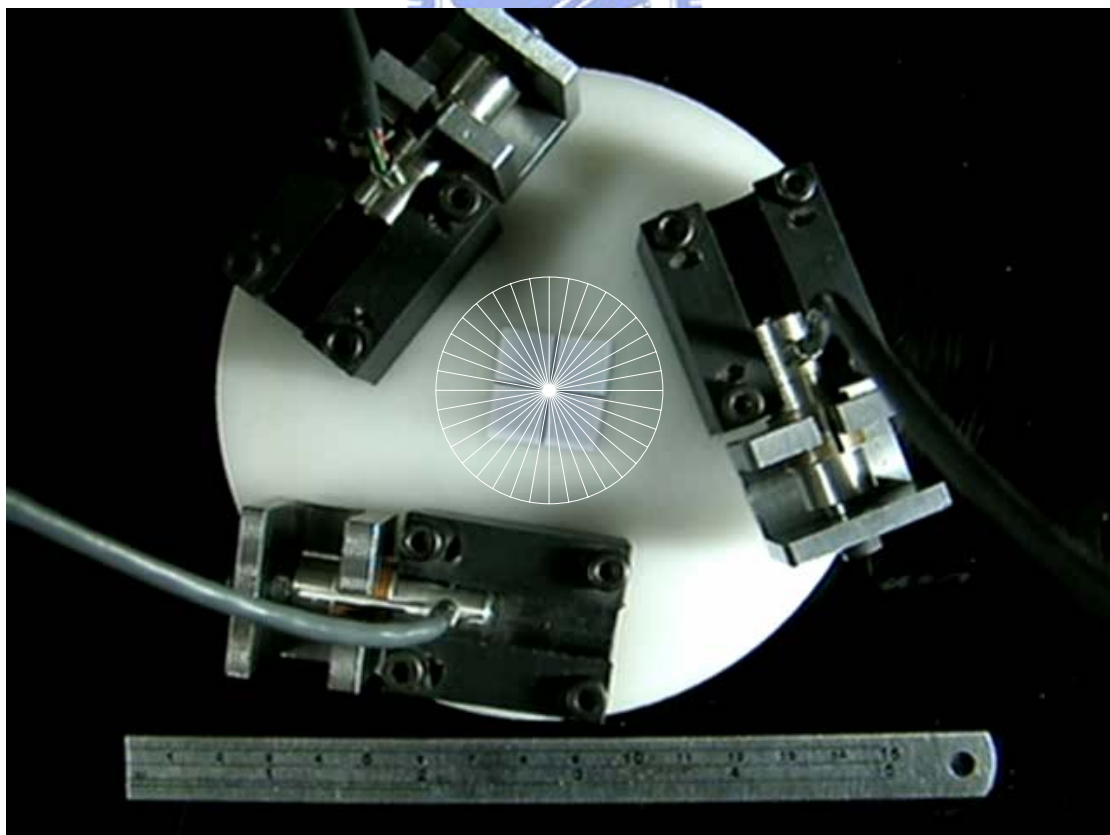Figure 4.14 The rotate diagram of 2-D IDM(second experiment)(a)0s(b) 30s
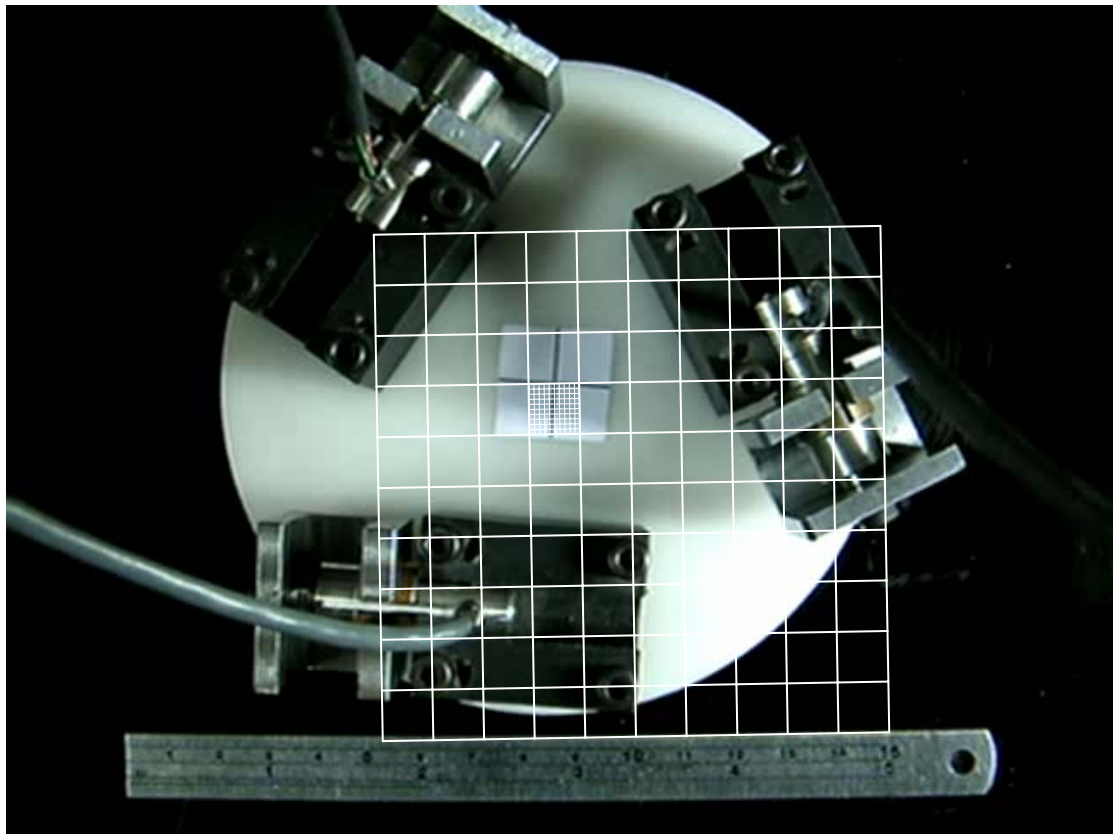
(a)
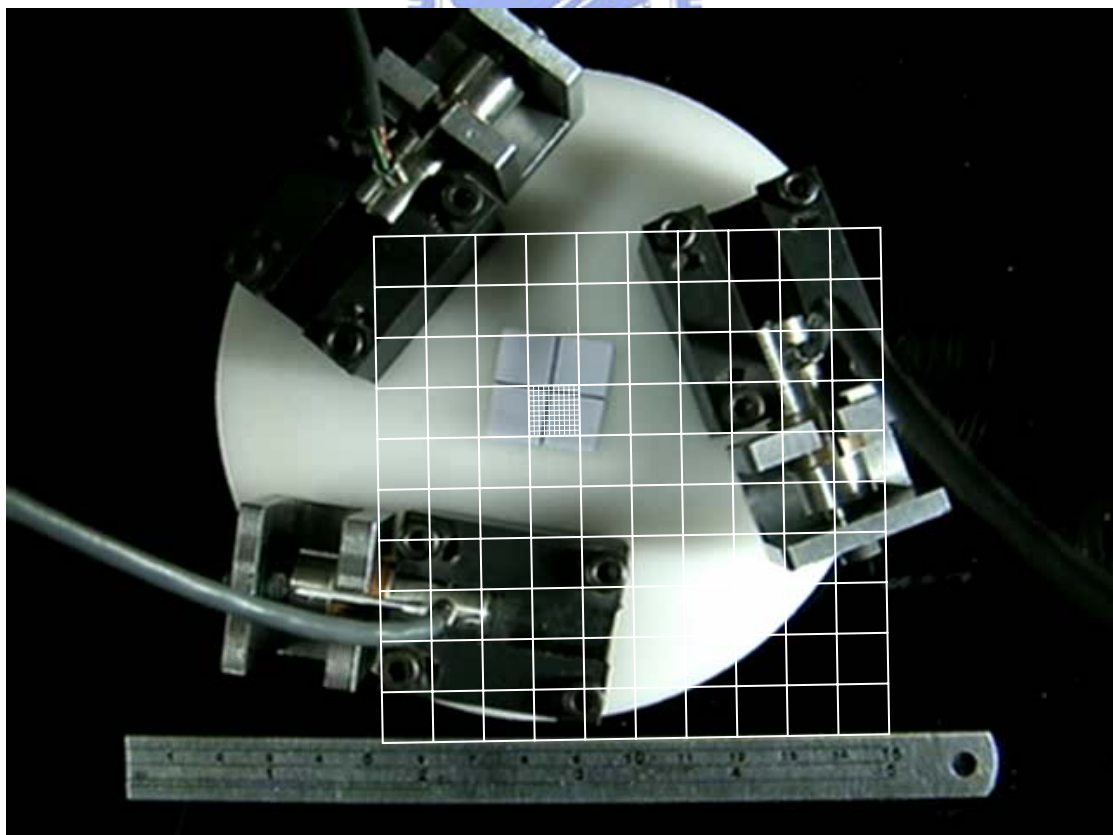
(b)

Figure 4.15 The grid diagram of 2-D IDM (third experiment)(a) 0s(b) 30s

(a)

(b)

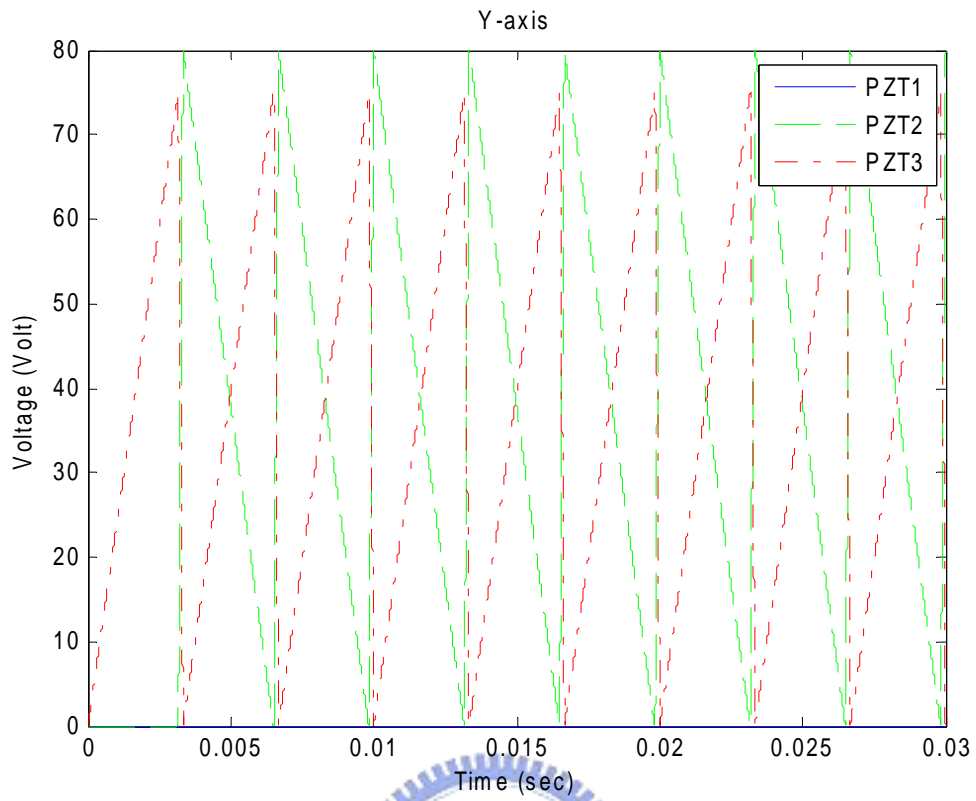Figure 4.16 The rotate diagram of 2-D IDM(third experiment)(a) 0s(b) 30s

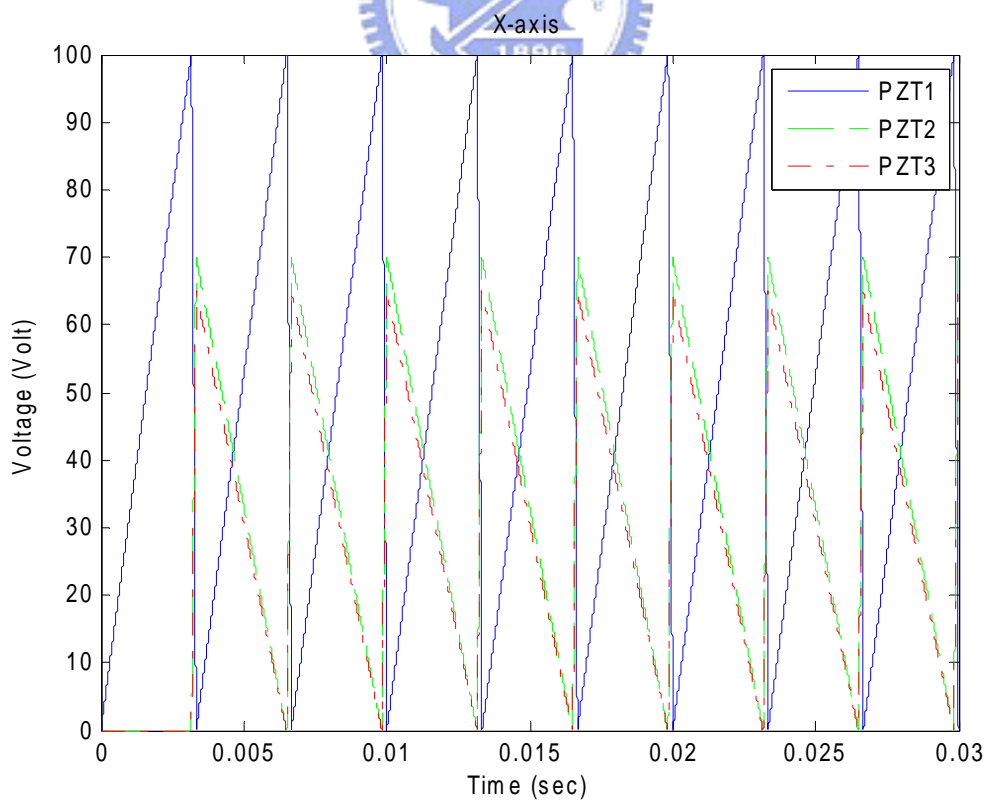Figure 4.17 Inputs of 2-D IDM about displacement in Y-axis

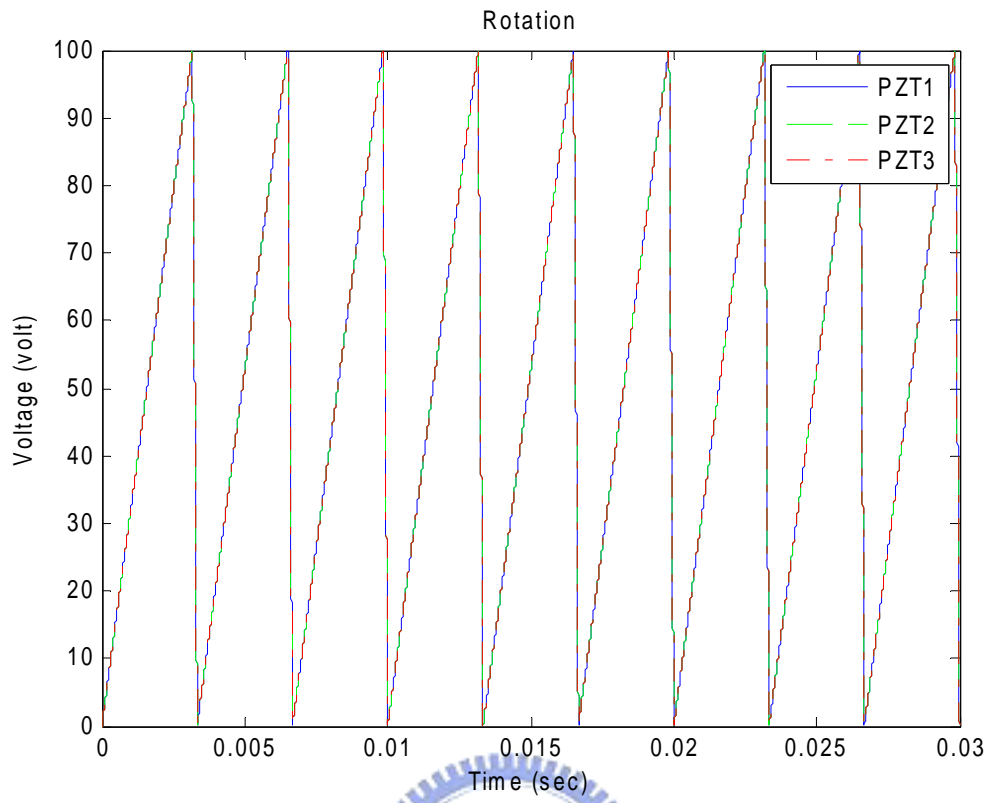Figure 4.18 Inputs of 2-D IDM about displacement in X-axis

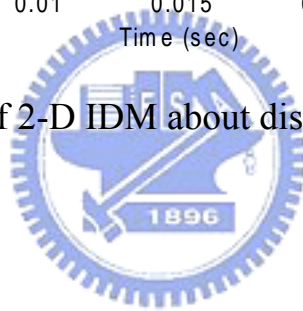Figure 4.19 Inputs of 2-D IDM about displacement in Rotation

M (Kg)	0.25
R (m)	0.062
m_1 , m_2 , m_3 (kg)	0.05
c_1 , c_2 , c_3 (N · t/m)	200
k_1 , k_2 , k_3 (N/m)	10^7
R_1 , R_2 , R_3 (m)	0.05
ϕ_1 (degree)	90
ϕ_2 (degree)	210
ϕ_3 (degree)	330
μ	0.3
I (kg · m^2)	0.0008

Table 3.1 The parameters of simulation

Model Number	PZL-015
Material	Lead zirconate titanate(PZT)
Type	Preloaded stack actuator with housing
Dimension	Piezo stack: rectangular disk 4mm╳5mm 0.25mm thickness PZT plate Total stack length: 20mm Housing: φ 12.7mm, length 33.8
Maximum Voltage	100V
Motion for 0~100V	10μm
Frequency Response	3.5KHz
Nonlinearity	4%
Hysteresis	15%
Creep	Increasing voltage: 1~2% in 20~30sec Decreasing voltage: 7~8% in 60~80 sec

Table 4.1 The specifications of Burleigh's piezoelectric actuator